

Understanding inverse metallicity gradients in galactic discs as a consequence of inside-out formation

Ralph Schönrich^{1★} and Paul J. McMillan^{2,1}

¹*Rudolf-Peierls Centre for Theoretical Physics, University of Oxford, 1 Keble Road, Oxford OX1 3NP, UK*

²*Department of Astronomy and Theoretical Physics, Lund Observatory, Lund University, Box 43, SE-22100 Lund, Sweden*

Accepted 2017 January 11. Received 2017 January 11; in original form 2016 May 8

ABSTRACT

The early stages of a galaxy’s evolution leave an imprint on its metallicity distribution. We discuss the origins and evolution of radial metallicity gradients in discs of spiral galaxies using an analytical chemical evolution model. We explain how radial metallicity gradients in stellar populations are determined by three factors: the radial metallicity profile of the star-forming interstellar medium (ISM), radial changes in the star formation history (in particular, inside-out formation) and radial mixing of stars. Under reasonable assumptions, inside-out formation steepens the negative ISM metallicity gradient, but contributes positively to the stellar metallicity gradient, up to inverting the metallicity profile to a positive $d[\text{Fe}/\text{H}]/dR$. This reconciles steep negative $d[\text{Fe}/\text{H}]/dR$ in some high-redshift galaxies to generally flatter gradients in local observations. We discuss the evidence for inverse radial metallicity gradients (positive $d[X/\text{H}]/dR$) at high redshifts and the inverse relationship between azimuthal velocity and the metallicity (positive $dV_\phi/d[\text{Fe}/\text{H}]$) of stars for the Milky Way’s thick disc. The former can be achieved by high central gas-loss rates and re-distribution processes, e.g. re-accretion of enriched material in conjunction with the inside-out formation and near-disc galactic fountaining. For the Milky Way-thick disc, we show that the positive $dV_\phi/d[\text{Fe}/\text{H}]$ correlation points to comparable time-scales for inside-out formation, initial metal enrichment and SNIa enrichment. We argue that the original ISM metallicity gradient could be inferred with better data from the high-metallicity tail of the alpha-enhanced population. Including inside-out formation in our models changes the local vertical metallicity gradient by about $-0.2 \text{ dex kpc}^{-1}$, in line with local measurements.

Key words: Galaxy: disc – Galaxy: evolution – Galaxy: kinematics and dynamics – galaxies: abundances – galaxies: evolution – galaxies: stellar content.

1 INTRODUCTION

This paper discusses the origins and temporal development of radial metallicity gradients in galactic discs as well as their imprint on local correlations between azimuthal velocities and metallicities. It is motivated by recent findings of inverse gradients in galactic discs: be it inverse radial metallicity gradients (i.e. positive $d[X/\text{H}]/dR$) found in external galaxies (Cresci et al. 2010), as well as inverse relationships between azimuthal speed and metallicity (i.e. positive $dV_\phi/d[\text{Fe}/\text{H}]$) for local thick disc stars (Spagna et al. 2010; Lee et al. 2011). These gradients are ‘inverse’ in the sense that they have opposite sign to those found in the present-day star-forming gas in disc galaxies, where metallicity decreases with radius (or equivalently, declines with angular momentum).

In contrast to young, thin disc populations, where the current metallicity gradient imprints a slower local mean rotation with increasing metallicity (see e.g. Casagrande et al. 2011), it was discovered by Spagna et al. (2010) and Lee et al. (2011) that the metal-poor, alpha-rich stellar population shows an inverse relationship between mean azimuthal speed and metallicity; i.e. in this subgroup, stars with lower metallicity show slower mean rotation than stars with higher metallicity. The increase of azimuthal velocity with metallicity has been confirmed for thick disc stars in Radial Velocity Experiment (RAVE) by Kordopatis et al. (2013). Curir et al. (2012) linked this to inverse metallicity gradients (i.e. larger metallicities in the outer regions of a disc) at early times, identified in the chemical evolution models of Spitoni & Matteucci (2011) and Chiappini, Matteucci & Romano (2001), as well as occasionally observed in high-redshift galaxies, such as those studied by Cresci et al. (2010).

The finding of Cresci et al. (2010) of a positive/inverted $d[\text{Fe}/\text{H}]/dR$ gradient at high redshift can also be linked to the finding of Queyrel et al. (2012), who found positive gradients

* E-mail: ralph.schoenrich@physics.ox.ac.uk

using nitrogen and oxygen emission lines in two isolated and apparently quiescent galaxies, which cannot relate to the strong gradient changes expected in mergers (Rupke, Kewley & Barnes 2010). Stott et al. (2014) find a similar picture, where metallicity gradients tend to be inverted or very small in galaxies with a high specific SFR. At the same time, e.g. Jones et al. (2010, 2013) have observed very steep radial metallicity gradients $d[X/H]/dR < -0.2 \text{ dex kpc}^{-1}$ in a few galaxies at redshift $z \gtrsim 2$, which, by far, exceed values measured in the Milky Way or other local galaxies. On the other hand, an analysis of the KMOS sample at redshifts in the range $z \sim 1\text{--}2.5$ (Wuyts et al. 2016) has yielded mostly flat radial abundance gradients in the gas phase (although with large scatter), as well as no significant correlation with structural parameters. We note that it is also very difficult to interpret these studies at current stage: most investigations rely on nebular oxygen and nitrogen lines, which are produced by various sources, ranging from active galactic nuclei (usually well controlled), through H II regions (associated with star formation) and planetary nebulae (linked to older stellar populations) to the warm/hot interstellar medium (ISM) itself.

Most work on the theoretical side has so far been performed with N -body simulations. In their first analysis of a cosmological disc simulation, Rahimi et al. (2011) reported stellar radial metallicity gradients of $d[\text{Fe}/H]/dR \sim -0.05 \text{ dex kpc}^{-1}$ in their intermediate-age stars and $-0.066 \text{ dex kpc}^{-1}$ in their young stars. Gibson et al. (2013) compare gradients in the ISM and stars of their simulations to the relatively steep negative gradients in cosmological observations from Jones et al. (2010) and Yuan et al. (2011). In the spirit of classical chemical evolution models (see e.g. Prantzos & Boissier 2000), which predicted a steepening in the ISM gradient due to the faster decline in SFRs in the central regions (which increases the ratio between yields and fresh accretion), Gibson et al. (2013) link the more negative gradient to the inside-out growth. However, we will show that while inside-out growth does tend to steepen the negative ISM gradient, it gives a positive contribution to the gradient in stars.

Both Sloan Extension for Galactic Understanding and Exploration (Cheng et al. 2012) and RAVE (Boeche et al. 2014) data have also pointed to a weakening of radial abundance gradients with Galactic altitude z , up to a mild gradient inversion, a behaviour that is also found in N -body models like that of Gibson et al. (2013). The inside-out growth of discs has been linked to the issue of gradients by several papers, e.g. Gibson et al. (2013), Minchev, Chiappini & Martig (2014) and Miranda et al. (2016). In particular, Minchev et al. (2014) link to inside-out growth the tendency of radial metallicity gradients to weaken and then invert with increasing altitude. However, they do not provide a detailed explanation of the mechanisms and causes, while Rahimi, Carrell & Kawata (2014) show a clear connection between flaring of younger populations towards the outer disc and the radial metallicity trend getting more positive with altitude. We will show that in our simulations, where we can separate the factors, this trend with altitude is linked mainly to radial migration and not to the inside-out formation.

To enter our discussion, it is important to note that the findings of inverse radial metallicity gradients (Cresci et al. 2010) are not directly equivalent to the inverse/positive relation between azimuthal speed and metallicity, discovered by Spagna et al. (2010). As a first obvious reason, older stars have been more affected by disc heating than younger ones, and this has opposite effects on the $R - [\text{Fe}/H]$ and $V_\phi - [\text{Fe}/H]$ gradients. If we hold the angular momentum distribution constant, heating the most metal-poor populations increases their mean Galactocentric radius (making the radial metallicity gradient more negative), while it increases asymmetric drift, giving

lower metallicity stars a comparably lower azimuthal velocity at a given radius (making the azimuthal velocity gradient more positive).

In this paper, we show that a clear discrimination between the origins of metallicity gradients in stellar populations is needed, and we identify and discuss the three major sources.

- (i) The time-dependent gradient in the star-forming ISM.
- (ii) inside-out formation and radial variations in the SFRs.
- (iii) Radial mixing of stellar populations.

We demonstrate that variations in the age distribution of the stars born at a given radius is just as important as the metallicity gradient of the star-forming gas at any time in the life of the galaxy in determining the final metallicity gradient of the stellar populations. Inside-out galaxy formation produces these variations in age and typically drives $d[\text{Fe}/H]/dR$ towards positive values, bringing very steep gradients at high redshift in line with a lack of such steep gradients in local disc galaxies. Radial migration by bars (Friedli, Benz & Kennicutt 1994) or spiral patterns (Sellwood & Binney 2002) also has a strong impact on disc structure and composition. However, local stellar data show that the mixing of all stellar populations in the disc of our Milky Way by this process is far from complete (Schönrich & Binney 2009a, hereafter SB09). We will show that the main effect of radial migration is to radially average and blur, but not completely destroy, these gradients.

In addition, we will discuss the likely sources of gradient flattening and inversions in the star-forming ISM, offering a slightly different perspective from the usual explanation that this is produced by low-metallicity accretion into the central regions.

This paper provides a more analytic discussion to disentangle the different observations and the processes that shape them. While our standard model is constructed to meet the main observables of the Milky Way, we do not attempt to produce a fiducial model for the Galaxy, and explicitly do not attempt specific fits to observations, which would be questionable given the uncertain errors and interpretation of measurements in the different surveys and, more importantly, would cloud the main incentive of this work. In Section 2, we quickly introduce two toy models/thought experiments to explain the problem of gradient formation. In Section 3, we quickly discuss the applied chemo-dynamic models, and in Section 4, we provide a short analytic framework to understand metallicity gradients in stars better, and discuss changes in radial abundance gradients, including a discussion of mechanisms to invert radial abundance gradients in the star-forming ISM. In Section 5, we discuss the relationships between chemistry and local azimuthal velocities, followed by a discussion of gradients at higher altitudes in Section 6. We conclude in Section 7.

2 TWO TOY MODELS

The key concepts explained in this paper can be readily understood by considering two toy models.

Consider the case of a galaxy that has a metallicity constant in radius at all times, but rising with time. If this galaxy forms inside out, i.e. if the ratio of SFRs between the inner disc (small L_z) and the outer disc (large L_z) is larger at small t , then today its lower metallicity stars will still be concentrated at smaller angular momenta. Or in other words, while at any time, the metallicity gradient of the star-forming ISM was zero, the galaxy in our thought experiment exhibits an inverse/positive radial metallicity gradient in its stars.

Secondly, consider the case where there is no radial gradient in the metallicity of the star-forming gas at any time during the evolution of

a galaxy, and no inside-out growth. Again, the older stars are more metal-poor, and have a higher velocity dispersion (because there is an age–velocity dispersion relationship). The more metal-poor stars therefore have higher velocity dispersions, and thus a larger asymmetric drift. This produces an inverse, i.e. positive gradient in the v_ϕ –[Fe/H] relation, while the associated radial expansion gives a small normal, i.e. negative contribution to the radial $d[\text{Fe}/\text{H}]/dR$ gradient.

In the following, we will discuss and quantify how these two effects alter gradients in the disc. In the next section, we will lay out the analytic chemodynamic models that we will use to compare the size of these effects, compared to the impact of other processes that shape these gradients, and will return to a more formal approach to this problem in Section 4.

3 METHOD OUTLINE

A quick definition of our use of ‘radial migration’ terms is necessary. Throughout this work, we define ‘radial mixing’ as the general re-distribution of stars born at some fixed angular momentum $L_{z,0}$ or corresponding radius to a position R , at which they are observed today. This radial mixing is conceptually split up into ‘churning’ (corresponds to the narrower meaning of radial migration), which re-distributes stars in angular momentum L_z , and ‘blurring’, which describes the re-distribution over different positions at fixed L_z caused by the excursions of stars along their orbits.

We use an improved version of the analytic chemodynamical galaxy models SMAUG (the models used by SB09). These models combine an analytical chemical evolution code with modelling of the galaxy’s dynamics, in particular, radial migration and the current kinematics and spatial distributions of stars. The model has two gas phases, warm/hot and cold. This allows us to account for the delays in metal enrichment; most of the processed material from dying stars is initially warm/hot, and needs to cool down and condense back into the star-forming cold ISM. The model machinery comprises full population synthesis in order to facilitate the replication of selection effects and to fully account for the time delay in enrichment. SMAUG also accounts for radial flows of the gas, including mixing from radial migration, inflow through the disc connected to accretion and a possibility for additional mixing. We have updated the approach to radial inflow with the angular momentum prescription from Bilitewski & Schönrich (2012). In addition, we have updated the kinematic modelling: we now assume both vertical and horizontal action conservation, implemented using the Torus Mapper (TM; Binney & McMillan 2016).

Otherwise, our assumptions here very much resemble those in SB09, resulting in a similar enrichment history (see Fig. 1). We use a radial resolution of roughly 0.25 kpc, and an increased time resolution of 15 Myr. The accretion history of the galaxy assumes the two-exponential inflow pattern applied in SB09: the disc is set up with an initial $10^8 M_\odot$ of primordial gas, and accretes $5 \times 10^{10} M_\odot$ with exponential decay time of 1 Gyr and further $1.0 \times 10^{11} M_\odot$ with exponential decay time of 9 Gyr. This shifts the accretion to slightly earlier times than in SB09, in concordance with cosmological expectations (see e.g. Wang et al. 2011), and other estimates for the star formation history, e.g. Aumer & Binney (2009). A large early accretion rate is also necessary to sustain high SFRs, while the inside-out-forming gas disc builds up its mass. As a result of the accretion, overall SFRs peak early and then slowly subside over the history of the system. The resulting scalelengths and local mass density near the Sun are comparable to estimates from observations (e.g. Holmberg & Flynn 2004; Flynn et al. 2006; Jurić

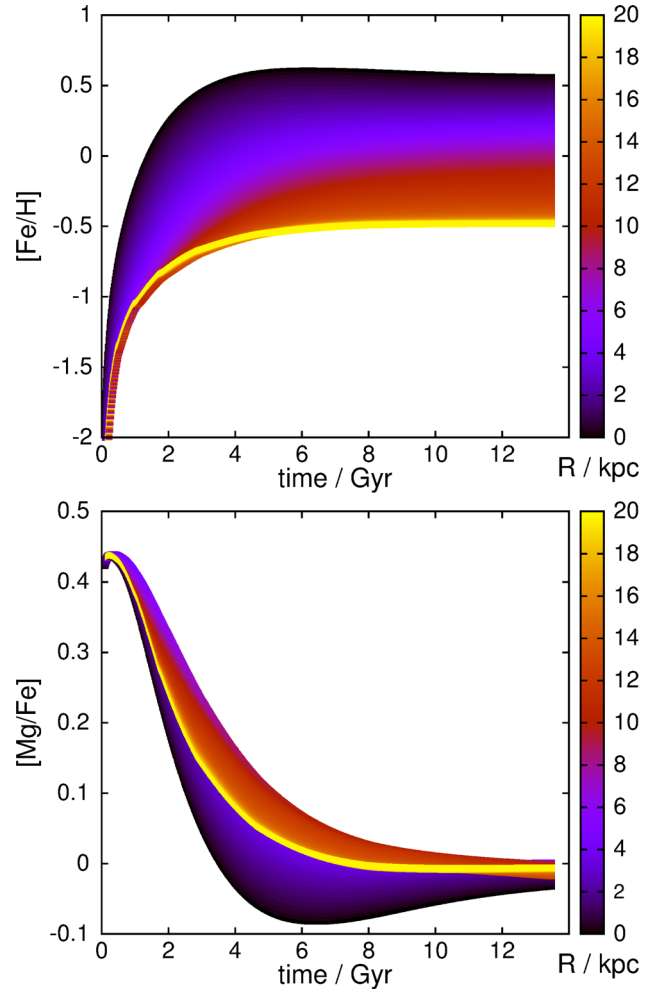


Figure 1. [Fe/H] and $[\alpha/\text{Fe}]$ of the star-forming gas as a function of time for the standard model with inside-out formation. Different colours correspond to different radii.

et al. 2008; Read 2014). In particular, the standard inside-out model has at $t = 12$ Gyr local surface mass densities of $36 M_\odot \text{ pc}^{-2}$ in stars and remnants, matching the derivation of McKee, Parravano & Hollenbach (2015), as well as $\sim 10 M_\odot \text{ pc}^{-2}$ in gas, slightly lower than the estimate of McKee et al. (2015), with a total baryonic mass of $5.0 \times 10^{10} M_\odot$. The total mass is significantly smaller than the accreted mass due to the mass-loss over time (see Section 3.3).

3.1 Inside-out growth and star formation

Inside-out growth in our simulations is applied by varying the scale-length of the exponential gas disc, R_g . When the galaxy accretes new mass at each time-step, setting the specific angular momentum of the infalling material leaves a degree of freedom, i.e. one can either specify the radial density profile of the infalling material or adapt the infall to approximate a shape of the targeted disc. We choose the latter option, keeping the gas disc exponential at all times while varying its scalelength. While it was shown in Bilitewski & Schönrich (2012) that reasonable inside-out growth does not significantly affect today’s metallicity gradients, its functional shape affects how the enrichment history populates the $[\alpha/\text{Fe}]$ –[Fe/H] abundance plane. We found that the simplest possible assumption, i.e. linear growth of the scale radius in time, up to a maximum value, is not viable. Any discontinuities in the growth rate create artefacts in the

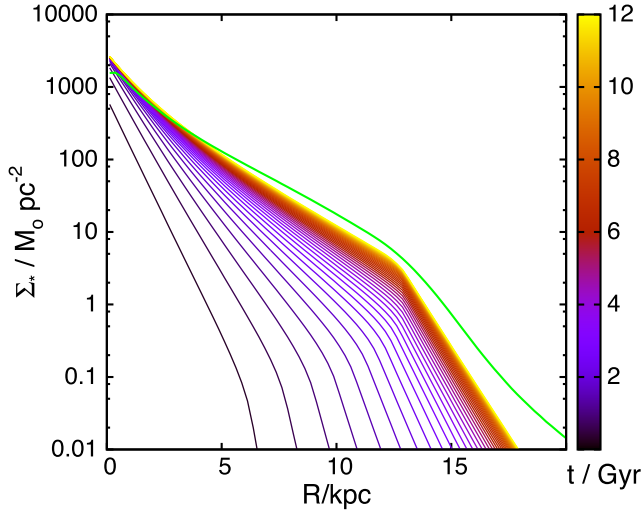


Figure 2. Radial stellar surface density profiles for the inside-out growing simulation when stars are kept fixed in angular momentum at their guiding centre radius, colour coded in time. This is equivalent to the integrated total star formation as a function of radius. The green line shows today’s density profile taking into account full radial mixing (churning and blurring).

metallicity plane and age–metallicity relation when the growth stops. We hence choose the fully differentiable function:

$$R_g(t) = R_{g,0} + (R_{g,e} - R_{g,0}) \times \left[\arctan\left(\frac{t-t_0}{t_g}\right) - \arctan\left(-\frac{t_0}{t_g}\right) \right] \times N, \quad (1)$$

where $R_{g,0}$ is the initial scalelength of the gas disc and $R_{g,e}$ is that after 12 Gyr. The normalization N is chosen to ensure that this condition holds at $t = 12$ Gyr. As a standard value, we use a growth time-scale $t_g = 2$ Gyr with an offset time $t_0 = 1$ Gyr, which implies near-linear growth of the disc during the first 2 Gyr and then a fast transition to a very slow growth of the scalelength. The standard inside-out model uses $R_{g,e} = 3.75$ and $R_{g,0} = 0.75$ kpc. We also note that the model’s recent growth rates are in line with estimates from Pezzulli et al. (2015).

For star formation, we use the Schmidt–Kennicutt law, i.e. the star formation efficiency is given by

$$\eta_{\text{SFR}} = 0.15 \left(\frac{\Sigma_g(t)}{M_\odot \text{ pc}^{-2}} \right)^{0.4} \text{ Gyr}^{-1}. \quad (2)$$

The pre-factor 0.15 is chosen to meet surface mass density and SFR constraints for the Milky Way; see also SB09. Note that the exponent of 0.4 in the star formation efficiency implies a shorter scalelength of the young stellar disc by a factor of 1.4 compared to the gas disc.

In this work, we assume a cut-off for the Schmidt–Kennicutt law: for a surface density below $4 M_\odot \text{ kpc}^{-2}$ in cold gas, we assume that the star formation efficiency drops with the third power of the gas surface density. We assume that stars inherit the elemental abundances of the cold ISM phase from which they are born without additional abundance scatter, motivated by the observations of very homogeneous abundances in young disc stars (see e.g. Przybilla, Nieva-F. & Butler 2008).

Fig. 2 shows the resulting development of the surface density of the stellar populations in time (colour coding), when neglecting churning and blurring, i.e. keeping stars at their radius of birth. This is equivalent to the integrated total star formation (minus lifetime effects) as a function of galactocentric radius. The cut-off in the

density profiles results from the applied cut-off in the Schmidt–Kennicutt star formation law (see above). The growth of the scalelength is evident, as well as initial accretion and scalelength growth of the disc move the outer star formation cut-off rapidly outwards at early times. At later stages, the growth of the gas-disc’s scalelength is partly balanced by the declining total gas mass of the disc, so that the cut-off radius for the star formation remains near $R \sim 14$ kpc. The thick green line shows today’s stellar surface density when fully accounting for radial migration (churning) and the random motions of stars (blurring). In particular, the latter term expands the disc, strongly increasing the surface densities in the outer disc and softening the stellar profile around the cut-off radius.

3.2 Model stellar dynamics

While SB09 approximated the vertical structure of the disc by isothermal distribution functions, with conserved vertical energy, the N -body simulations of Solway, Sellwood & Schönrich (2012) showed that it is the vertical action that is (on average) conserved by stellar migration. (The simulations of Vera-Ciro et al. 2014 suggest that this may not be completely true if there is very violent spiral activity.) We therefore employ the quasi-isothermal distribution functions of Binney & McMillan (2011) in the potential by Piffl et al. (2014), which replace the old isothermal distribution in energy $\exp(-E/\sigma^2)$ with the action distribution $f(J_i) \propto \exp(-(v_i J_i)/\sigma_i)$.

We use the same age–velocity dispersion relations as in SB09, which are closely related to the usual power-law dependence on time found in the solar neighbourhood e.g. by Dehnen & Binney (1998), Holmberg, Nordström & Andersen (2009) and Aumer & Binney (2009):

$$\sigma_i = \max \{ \sigma_{i,\min}, \sigma_{i,10} (t/10 \text{ Gyr})^\beta \}, \quad (3)$$

where $\beta = 0.33$ is the usual time-exponent. Strictly speaking, the parameters σ_i are not the local dispersions, but are closely linked to them.¹ Since this equation uses the epicycle frequencies ν_i at the guiding centre radius, and since actions diverge when velocities approach the escape speed, cutting the wings in the velocity distribution short compared to a Gaussian, the velocity dispersions are of the order of ~ 10 per cent smaller than the parameters σ_i in the relevant areas of parameter space. We use the epicycle frequencies of each population’s birth radius, and keep their action distributions for each population fixed, no matter how migration has changed their guiding centre radii.

Accounting for this effect, we use $\sigma_{z,10} = 28$ and $\sigma_{R,10} = 43 \text{ km s}^{-1}$ for stars born in the solar neighbourhood. Following the traditional approximation of analytic kinematic models (which, among other benefits, approximates a constant scaleheight of coeval local populations; see also SB09 and Piffl et al. 2014, for references), we assume an exponential behaviour of $\sigma_{i,10}(R)$, i.e. $\sigma_{i,10}(R) = \sigma_{i,10}(R_0) \exp(-R/R_{\sigma_i})$ with galactocentric radius, and let the dispersion parameters decrease exponentially towards larger radii with scalelengths $R_{\sigma_i} = 5$ and 7.5 kpc, respectively (i.e. 2 and 3 disc scalelengths), setting a minimum dispersion of $\sigma_{\min} = 7 \text{ km s}^{-1}$ for the youngest stars.

For each group of coeval stars born at some radius/angular momentum ($R_0/L_{z,0}$), we hold their action distributions constant regardless of their radial migration. To avoid eventual problems with

¹ We will use the term ‘kinematic heat’ to refer to the spread in radial and vertical actions. This is closely related to the velocity dispersion, but not identical.

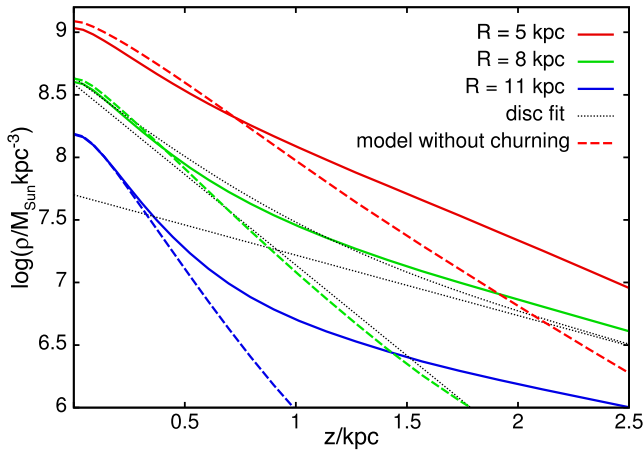


Figure 3. Vertical density profiles at different radii. For comparison, we show a common two-exponential decomposition into $\exp -z/(0.3 \text{ kpc}) + 0.13 \exp -z/(0.9 \text{ kpc})$ (grey lines). The dashed lines show the vertical density profiles we would have if there was no radial migration (i.e. populations kept their initial angular momentum).

the epicycle frequencies and kinematics of innermost stars, we use the action distributions of $R = 1.5 \text{ kpc}$ for all stars with $R < 1.5 \text{ kpc}$; however, we checked that this cut-off does not significantly affect our results.

Fig. 3 shows that the model disc (with solid lines) has scaleheights comparable to those of the Milky Way, and shows a thin/thick disc structure. While we did not attempt to fit the Milky Way profile, the model at $R \sim 8 \text{ kpc}$ fits quite closely the two-exponential fits from Ivezić et al. (2008) and Jurić et al. (2008). With black dashed lines, we show the decomposition $\exp(-z/(0.3 \text{ kpc})) + 0.13 \exp(-z/(0.9 \text{ kpc}))$.

We further assume that the extent of the migration (churning) of a star is independent of its current actions, which is approximately justified by the results of the N -body simulations of Solway et al. (2012). This is challenged by the results of Vera-Ciro et al. (2014) who found that migrated stars make up a population with a lower initial vertical velocity dispersion than those that do not migrate (implying that typically stars with low vertical actions are more likely to migrate). The difference between the two results is probably due to the Solway et al. (2012) simulations being dominated by low- m mode spirals, while those of Vera-Ciro et al. (2014) are dominated by multi-armed (high- m) spiral patterns. Our choice to assume that the migration coefficients are independent of current actions is motivated by our preference of not to complicate the picture here, as the effect of migration is, mostly, to average and weaken the observed gradients that we are interested in. Minchev et al. (2012) claimed that the prevalence of average action conservation instead of vertical energy conservation is the reason why they do not see thickening in their simulated disc under migration (the idea of migration thickening outwards migrating populations was first proposed in Schönrich & Binney 2009b, hereafter SB09b). Minchev et al. (2012) unfortunately convolute the question of heating with migration. Migration does not heat the disc, it just transfers stars with potentially wider action distribution from the inner disc. We can quantify analytically that outwards migrating populations under action conservation achieve larger scaleheights (see equation 27 in Schönrich & Binney 2012). Consistently, this has been shown in simulations, implicitly in Loebman et al. (2011), and with an explicit investigation by Roškar, Debattista & Loebman (2013), refuting the claims in Minchev et al. (2012). This model shows that under action

conservation, we even obtain a slightly thicker disc than measured locally in the MW, while the comparison case without radial migration (dashed lines in Fig. 3) shows no sign for any thick disc. Hence, it is clear that outwards migrating populations can thicken sufficiently under action conservation. The central question here is, however, not the effect of action conservation, but instead: (i) How large is the effect of preferential migration of kinematically colder subsets? (ii) Can secular processes provide sufficient kinematic heat in the inner disc regions, or do we require mergers. For the latter, it has been shown that molecular clouds with a fixed mass distribution do not provide sufficient heating in the inner disc (Aumer, Binney & Schönrich 2016). It remains to be tested how much impact a changing mass distribution can have, and also whether the time-dependent heating for each population needs a more sophisticated recipe in future models.

The radial dependence of migration is formulated as in SB09. We assume a maximum exchange fraction between neighbouring rings of 0.2 per half-time-step (i.e. 7.5 Myr). Note that this mass exchange between neighbouring rings conserves the detailed angular momentum balance, i.e. churning itself does not expand the disc.² Most of the expansion of the disc stems from blurring – as the stellar populations heat up, they move on orbits with larger mean radii than circular orbits with the same angular momentum.

3.3 Model chemical evolution

The chemical evolution is treated as in SB09, with the small difference that we are not using a fixed metallicity for the infalling gas. While it is unclear what metallicity freshly accreted gas had in the early Milky Way, a value close to today's value (near $[\text{Fe}/\text{H}] \sim -0.6$), as assumed in SB09, creates an inwards travelling metallicity wave with an inverse metallicity gradient at early times: the freshly arriving gas has a higher metallicity than the currently present gas, and the inner galaxy is better shielded against this infall due to its larger mass density and higher mass-to-infall ratio. This can increase metallicities in the outer regions much faster than the native enrichment in the inner regions, and hence creates inverse radial metallicity gradients. While we consider this possible scenario that strong outflowing winds carry large amounts of stellar yields above the disc, from where they can be re-accreted also on to the outer parts of the disc (especially in light of suspecting galactic fountaining; see Marinacci et al. 2011; Brook et al. 2012), more natural and likely than the explanation with cold inflows penetrating mainly to the centre of Cresci et al. (2010), it is not our main subject of study here. What we need for the model is to track a reasonable composition of the inflow and a smooth development of its metallicity. To keep things simple, we use the composition of the cold gas at the current stellar half-mass radius of the model, and scale its metallicity as $Z_t \tan^{-1} Z_t/Z_s$, where $Z_s = 0.25 Z_\odot$ and Z_t is 0.4 times the metallicity at the half-mass radius. The metallicity of hereafter SB09b the accreted material is of lesser importance to our models, since it mostly sets the metallicity of outer disc stars that have a minor impact on local samples. Our assumption is an educated guess from reviewing literature on the Milky Way's high-velocity clouds (see e.g. Collins, Shull & Giroux 2007; Shull et al. 2011) that have metallicity measurements ranging somewhere between 0.1 and

² The one exception to this is due to the participation of the gas disc in the same process. Since the gas disc has a longer scalelength, exchange of angular momentum between gas and stars will cause a mild radial expansion of the stellar populations. This is of particular importance near the cut-off.

$0.55 Z_{\odot}$. The highest values are found for the Smith cloud currently merging with the Galactic disc (Fox et al. 2016), consistent with a simple expectation of a mild increase of metallicity by interaction with the more metal-rich outflow of the Galaxy. Our main concern is that our prescription ensures a smooth rise of the infall metallicity, ending slightly above one quarter solar metallicity.

For the galactic gas, we keep the two-phase model of SB09. We now use as our standard initial mass function (IMF) the Chabrier (2003) IMF instead of the Salpeter (1955) IMF. This increases the ratio between high-mass stellar yields and the lock-up in low-mass stars by a large factor that needs to be balanced by a higher loss rate to inter-galactic medium (IGM) in concordance with the results from cosmological observations, as well as theoretical expectations and simulations (e.g. Meyer & York 1987; Aguirre et al. 2001; Davé et al. 2001; Nath & Trentham 1997). In particular, Tumlinson et al. (2011) find that the amount of metals in the circumgalactic gas likely surpasses the amount held in galactic discs, i.e. those galaxies have lost more than half the stellar yields.

In the model, we have two ways of implementing a metal loss. Either by a direct loss of stellar yields, or by a mass load parameter η_1 , i.e. for every unit mass of star formation, η_1 unit masses of gas are lost from the gas disc. At the same equilibrium metallicity, the latter term has a tendency to induce a quicker early enrichment, since it evaporates larger amounts of the present metal-poor gas and loses less early stellar yields. Both parameters are degenerate in fitting today's metallicities, but we can fix the total loss using today's local ISM metallicity. To allow for a somewhat enriched outflow, we use a direct loss fraction of stellar yields of 0.45, coupled to a mass load parameter of $\eta_1 = 0.45$. This parameter set is equivalent to a direct loss of 0.66 of stellar yields (a Salpeter IMF would require 0.1; for an extended discussion of IMF impacts, see Andrews et al. 2016).

There will be a difference in the re-distribution of yields from core collapse (SNII) supernovae and SNIa. Most core collapse SNe will happen within the dense star-forming ISM, while the time-delay of SNIa allows their progenitors to leave the dense regions. This raises the expectation that core collapse SNe give back more yields directly to the cold gas phase, while most of the SNIa yields will go to the warm/hot ISM. We also know that the Solar system was enriched with radioactive elements (partly r-process), e.g. Curium 247 (see e.g. Tissot, Dauphas & Grossman 2016) with lifetimes of the order of 10 Myr that demands a fast entrance of yields into the star-forming ISM. In rough concordance with the simulations of Walch et al. (2015), we split the retained yields from massive stars equally between the cold and the hot ISM, while for SNIa, we only add 1.5 per cent directly to the cold phase. With the same argumentation, we set the time constant for the freeze-out of the warm/hot gas to the cold phase to 1 Gyr, yielding a total mass in the warm/hot phase of $10^9 M_{\odot}$ today. The precise freeze-out time-scale is of minor importance to our results. Its main effect here is to delay the initial enrichment of the cold gas, and hence degenerate with uncertainties in the early loss rates. We discuss its influence on the stellar metallicity gradient in the inner disc in Section 5.

3.4 Gas inflow and mixing

The re-distribution of gas within the galaxy is of great importance. For the inflow through the disc, we use the prescription of Bilitewski & Schönrich (2012), which is in concordance with a different formulation used by Pezzulli & Fraternali (2016). This prescription assumes that gas accretion on to the disc dilutes the angular momentum of the disc (see Lacey & Fall 1985) and drives

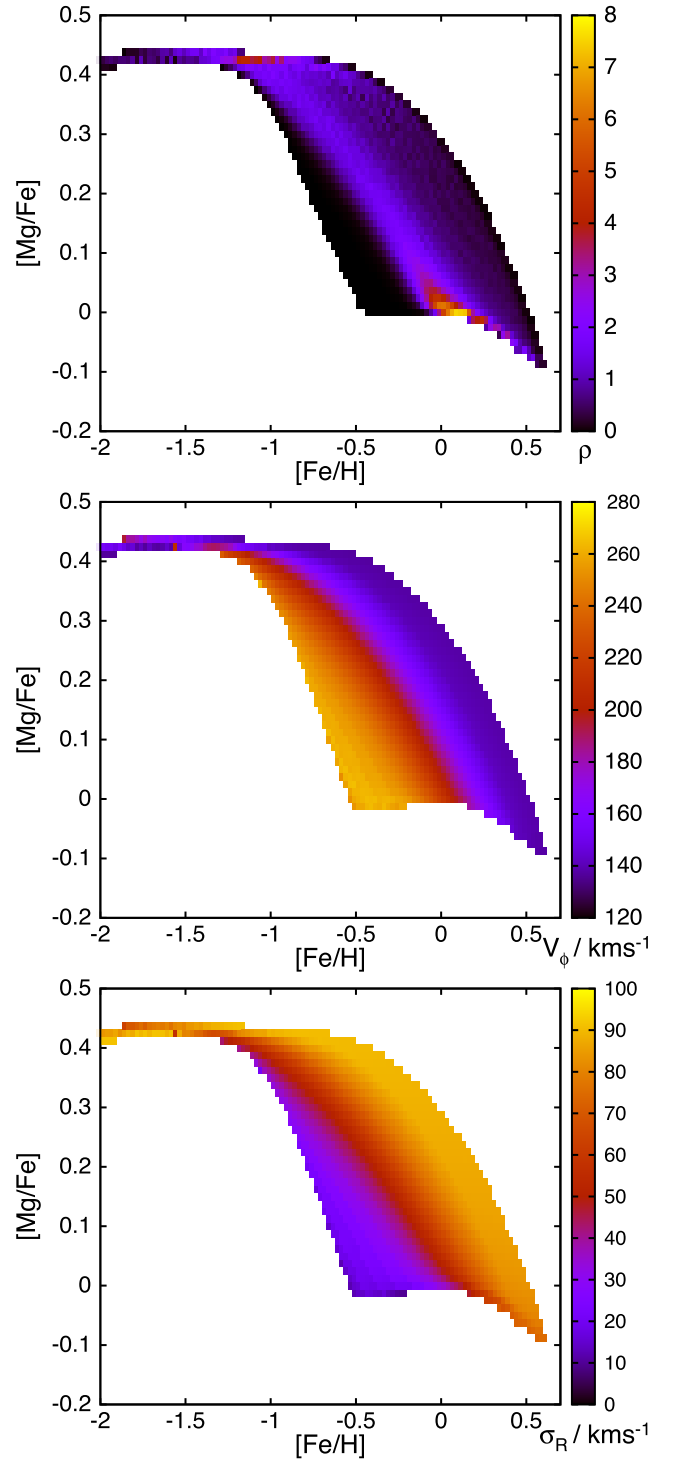


Figure 4. Densities, mean azimuthal velocities and radial velocity dispersions in the metallicity plane at $R = R_0$, $z = 0.4$ kpc.

the disc gas inwards, while conserving total angular momentum. The parameters are constrained by fitting the resulting radial metallicity gradient in the star-forming ISM to the observed gradient in Cepheids (Luck & Lambert 2011). For the angular momentum of the accreted gas, here we use 0.35 in the centre, rising linearly to 0.85 at the outer edge at 25 kpc.

As can be seen from Figs 1 and 4, the structure of the disc in the age–chemistry–kinematic space still largely resembles the older

versions of this model (see SB09, fig. 6; SB09b, Fig. 1 ff.). The vertical density profile shows the classic two-exponential behaviour, though this is less pronounced in the inner disc, because the model has no explicit bulge or bar, and outwards migrating stars need approximately a scalelength or more to thicken/flare up sufficiently. Fig. 1 shows $[\text{Fe}/\text{H}]$ and $[\alpha/\text{Fe}]$ versus time at each radius (colour coded). We note the relatively quick initial enrichment, followed by the transition into a nearly stable state, comparable with the results from Haywood (2008), the GCS survey (Casagrande et al. 2011) and the *Gaia*-ESO survey (Bergemann et al. 2014). Fig. 4 shows the overall density, mean azimuthal velocity and radial velocity dispersions as a function of position in the metallicity plane at $R = R_0$, $z = 0.4$ kpc.

In addition to the inwards flow, gas is re-distributed and mixes throughout the galaxy. As a minimum estimate of this diffusion, we assume the same radial migration for gas as for young stellar populations. However, the mixing may be much larger due to the turbulent diffusion. It is also reasonable to believe that yields in the warm/hot gas phase might experience different (stronger) mixing and therefore more re-distribution than the cold gas phase. Some models have played with re-distribution of yields, e.g. launching yields as compact clouds on ballistic trajectories from the disc (see e.g. Spitoni, Recchi & Matteucci 2008), but the observational and theoretical constraints for the properties of the hot phase are unsatisfactory. In principle, the disc will also lose some angular momentum to the warm/hot phase, driving a bulk of stellar yields outwards; the balance from stellar yields alone would be of the right order to cancel the metallicity gradient created by the inflow. However, it is not known how this warm/hot medium interacts in turn with the corona and with the inflow into the galaxy.

Our ‘standard’ model does not include additional gas mixing, but for this study, we will test the simplest and most conservative possible additional mixing model, leaving the radial density distribution of the Galactic gas untouched. This can be achieved by constructing the mixing process out of small, mass conserving interchanges of gas between neighbouring rings:

$$\Delta m_{i \rightarrow i+1} = k \sqrt{m_{i+1}/m_i} \quad \Delta m_{i \rightarrow i-1} = k \sqrt{m_{i-1}/m_i}, \quad (4)$$

where m_i is the mass residing in ring i , and k is a parameter setting the mass transition. For the innermost rings where there are large mass ratios between neighbouring rings (because rings of equal radial width have very different areas), we limit k , such that the exchanged mass does not exceed the mass in each ring. Stronger mixing can now be achieved by changing the parameter k and re-distributing the mass several times per time-step (the effective mixing length will be proportional to the square-root of the number of steps). In our model variant with additional gas mixing, we use eight substeps (so an exchange between neighbouring rings every ~ 1 Myr), and let $k = 0.3$ in the first 6 Gyr, then decaying exponentially with time-scale 6 Gyr.

3.5 Main models used

Unless otherwise stated, we evaluate the properties of all models after 12 Gyr, at $(R, z) = (8.3, 0.7)$ kpc with a mass-weighted selection function.

The three model variants we typically compare are: the ‘standard’ inside-out model (which we refer to as inside-out), a constant scalelength model, with the sole difference of a constant gas disc scalelength (no-inside-out) and the inside-out model with additional gas mixing (IO+MIX).

4 DISENTANGLING THE DRIVERS OF METALLICITY GRADIENTS

Most of the previous discussions of inverse metallicity gradients in disc populations have focused on an inverse gradient in the star-forming gas or youngest stellar populations, i.e. considerations of the metallicity profile in galactocentric radius $[\text{Fe}/\text{H}](R, t)$ or $Z(R, t)$ at a given point in time t . However, for an adequate discussion, one has to take into account the full star formation history and re-distribution of stars. We have to relate the abundances found at the time of our measurement t_m at position R to the past star formation all over the disc. We let stellar populations originate at angular momenta $L_{z,0}$, which correspond to the radii R_0 of a circular orbit; however, using $L_{z,0}$ is more natural to radial migration and leaves the door open to account for the slight adiabatic shrinking of the galaxy.

Different measurements of metallicity profiles are all related but logically distinct. The basis of the stellar profiles at later times is the original, time-dependent metallicity profile in the cold ISM, $Z_b(L_{z,0}, t)$, which we will refer to as ‘ISM gradient.’ The time-integral of the ISM gradient times the star-formation rate gives then the ‘star formation averaged metallicity gradient in the star-forming gas’, which would be a naive predictor for the stellar metallicity profiles at a later time, but is altered by stellar migration, described by a time-dependent mapping (Blurring + Migration) $T = B \cdot M$ between original angular momentum and final position. Throughout this section, we will use abbreviated notation for all differentials, i.e. $d_R \equiv d/dR$ and $\partial_R \equiv \partial/\partial R$.

The expectation value for the metallicity of stars found at a certain radius R at time t_m can be described by

$$\langle Z(R, t_m) \rangle = W(R) \iiint Z_b(L_{z,0}, t) G(L_{z,0}, t) M(L_{z,0}, L_z, t) \times B(L_{z,0}, L_z, R, t) dt dL_z dL_{z,0}, \quad (5)$$

with normalization W , time of birth of each population t , original angular momentum $L_{z,0}$, angular momentum L_z at time of measurement t_m and current position R . The time integral runs from the birth of the disc (0) to t_m .

The four terms under the integral sign are as follows.

- (i) $Z_b(L_{z,0}, t)$: the metallicity of the stars born with angular momentum $L_{z,0}$ at a time t , inherited from the star-forming ISM at the radius R_0 of the circular orbit with angular momentum $L_{z,0}$.
- (ii) $G(L_{z,0}, t)$: the SFR at radius R_0 and time t .
- (iii) $M(L_{z,0}, L_z, t)$: the transition matrix in angular momentum. Stars born with angular momentum $L_{z,0}$ have a probability $M(L_{z,0}, L_z, t)$ to migrate to the current angular momentum L_z , i.e. ‘churning’.
- (iv) $B(L_{z,0}, L_z, R, t)$ is the probability of finding a star with angular momentum L_z at a radius R . This describes ‘blurring’: by the excursions along their orbits, stellar populations with current angular momentum L_z are distributed over a range of radii and altitudes (R, z) . The term also depends on t and $L_{z,0}$.

We note that for matching observations, all equations would have to carry a selection function that will depend on the radius of birth (and hence metallicity), the age of each population and, for most surveys, on the current position in the galaxy. This will again alter the observed metallicity profiles. For this paper, the accounting for selection would complicate the picture without providing any further insight.

To simplify equation (5), we contract churning and blurring: no other variable depends on the current angular momentum of the stars, so we can execute the integral over L_z and obtain the new map

$T(L_{z,0}, R, t)$, which is the probability that a star born at $(L_{z,0}, t)$ is now at position R

$$\langle Z(R, t_m) \rangle = W \iint Z_b(L_{z,0}, t) G(L_{z,0}, t) T(L_{z,0}, R, t) dt dL_{z,0}. \quad (6)$$

The normalization $W(R, t_m)$ is simply the number of stars present at R , i.e.

$$W(R) = \left(\iint G(L_{z,0}, t) T(L_{z,0}, R, t) dt dL_{z,0} \right)^{-1}. \quad (7)$$

Note that the mass conservation normalizes T , such that:

$$\int T(L_{z,0}, R, t) dR = 1 \quad (8)$$

The task is to understand today's metallicity gradient $d/dR \langle Z(R, t_m) \rangle$. However, we did not find it very instructive to directly differentiate equation (6). To gain a better intuition, we introduce the normalized star formation history at each radius/angular momentum

$$g_*(L_{z,0}, t) = G(L_{z,0}, t) (S_g)^{-1} = G(L_{z,0}, t) \left(\int G(L_{z,0}, t) dt \right)^{-1}. \quad (9)$$

where $S_g(L_{z,0})$ is the time-integrated star formation density at some original angular momentum $L_{z,0}$. Now,

$$\langle Z \rangle = W \iint Z_b g_* S_g T dt dL_{z,0}. \quad (10)$$

We can further absorb the local normalization $W(R)$ into T , resulting in a new T' , so our equation reads:

$$\langle Z \rangle = \iint Z_b g_* S_g T' dt dL_{z,0}. \quad (11)$$

Note that instead of the old normalization condition for W and the mass conservation on T , we now have the normalization condition

$$\iint g_* S_g T' dt dL_{z,0} = 1. \quad (12)$$

We can therefore straightforwardly interpret $(g_* S_g T')(L_{z,0}, R, t)$ as the normalized distribution of birth angular momentum and birth dates of all objects now found at radius R .

Differentiating equation (11) with the help of Leibniz' rule, we obtain

$$d_R \langle Z \rangle = \iint Z_b g_* S_g \partial_R (T') dt dL_{z,0}. \quad (13)$$

This is interesting, because the classic way of thinking about metallicity distributions as the cumulated abundance gradient in the star-forming gas does not appear here (no spatial derivative of Z_b). The abundance gradient in the present stellar populations is determined by the distribution of origin of stars at a given radius (both in time and initial angular momentum). This depends on the star formation and enrichment history, as well as the radial re-distribution.

To assess the situation, we need to link this equation to the original gradients, i.e. we need to recover a derivative in the radius of birth, or better original angular momentum $L_{z,0}$: we split the radial mixing term $T = T_1 + T_2$ into a 'trivial/well-behaved' part T_1 that does not change the re-distribution function with radius, i.e. $T_1(L_{z,0}(R_1), R_2, t) = T_1(L_{z,0}(R_1 + \delta R), R_2 + \delta R, t)$, and a part T_2 that does change with $L_{z,0}$ (and covers the more complicated/higher order aspects of radial mixing). With the simple assumption of a constant rotation speed V_c , the condition for T_1 implies:

$$\partial_R T_1 = -V_c \partial_{L_{z,0}} T_1. \quad (14)$$

We define T'_1 just as before by absorbing $W(R)$ into T_1 . Inserting equation (14) into equation (13),

$$d_R \langle Z \rangle = - \iint Z_b g_* S_g (V_c \partial_{L_{z,0}} T'_1 - T_1 \partial_R W) dt dL_{z,0} + \iint Z_b g_* S_g \partial_R T'_2 dt dL_{z,0}, \quad (15)$$

where the second term in the first line comes from the definition of T'_1 . Since, $S_g = 0$ both for $R = 0^3$ and $R \rightarrow \infty$, so that we can integrate by parts, i.e.

$$\iint Z_b g_* S_g (V_c \partial_{L_{z,0}} T'_1) dt dL_{z,0} = - \iint T'_1 \partial_{L_{z,0}} (Z_b g_* S_g) dt dL_{z,0}. \quad (16)$$

Regrouping our terms from the first line, we obtain

$$d_R \langle Z \rangle = \iint V_c S_g T'_1 (g_* \partial_{L_{z,0}} Z_b + Z_b \partial_{L_{z,0}} g_*) dt dL_{z,0} + \iint Z_b g_* (V_c T'_1 \partial_{L_{z,0}} S_g + S_g T_1 \partial_R W) dt dL_{z,0} + \iint Z_b g_* S_g \partial_R T'_2 dt dL_{z,0}. \quad (17)$$

We will see that this has broken down today's stellar metallicity gradient profile into three basic concepts: the star-formation averaged metallicity gradient (first term), and two terms widely neglected in the literature, the impact by SFR profile changes/SFR part of the gradient (second term) and some rather annoyingly convoluted terms caused by migration (second and third line).

The first line links directly to the original star formation history, but it consists of two terms: the inherited star formation weighted metallicity gradient $g_* \partial_{L_{z,0}} Z_b$ and the metallicity weighted star formation gradient $Z_b \partial_{L_{z,0}} g_*$. We can intuitively see that these two terms will be of the same order and, in most cases, have opposite signs. The first term is typically of the order of $-0.05 \text{ dex}/(\text{kpc} V_c)$, while the second term links ~ 1 dex of enrichment with time to the temporal change of the SFR. This temporal change (in particular, in the inner disc regions) in the fraction of metal-poor stars formed early on, will easily exceed $\gtrsim 0.1$ between the inner and outer radii, hence giving positive radial contribution of the order of $\sim 0.1 \text{ dex}/(\text{kpc} V_c)$ to the stellar metallicity gradient. In simple words: if there is strong inside-out formation on a time-scale comparable to the enrichment time-scale, and if a significant number of stars are formed during that phase, the overall metallicity gradient of the stellar populations in a galaxy can be inverted. T'_1 in the first line fulfills the zeroth-order contribution of radial mixing: it makes the gradient term from the first line just the average of all regions contributing to the stellar populations found at R .

The second line in equation (17) balances the density gradients in the disc. If there is no radial mixing, then T' approaches an identity map, i.e. $T'_1 \rightarrow \delta(L_{z,0} - R V_c)$. In that case, $W \rightarrow S_g^{-1}$ and the second line vanishes, as well as the third line, which summarizes the irregular part of radial mixing.

Having understood the nature of the three major players for today's abundance gradients (time-dependent ISM gradient, SFR differences radial mixing), we can now split them conceptually apart.

³ This is fulfilled by definition. $S_g(R) = \int_0^{2\pi} \Sigma_*(R, \phi) d\phi$, where Σ_* is the time-integrated star formation surface density that is, by construction, finite. If we formulated this in $L_{z,0}$, the same argument would hold as long as $\lim_{R \rightarrow 0} V_c(R) > 0$.

In the absence of radial mixing, the integral in $L_{z,0}$ in the first line of equation (17) disappears, so that we can divide

$$\begin{aligned} (d_R \langle Z \rangle) &= (d_R \langle Z \rangle)_{\text{nomix}} + (d_R \langle Z \rangle)_{\text{mix}} \\ &= V_c \int g_* \partial_{L_{z,0}} Z \, dt + V_c \int Z \partial_{L_{z,0}} g_* \, dt + (d_R \langle Z \rangle)_{\text{mix}}. \end{aligned} \quad (18)$$

Fig. 5 summarizes this, showing the three parts: (i) the star formation-averaged metallicity gradient in the star-forming gas (green, first term of equation 17), (ii) the change in the age distribution of stars with radius (blue, second term in equation 17) and (iii) changes via the radial mixing of stars (red, all other terms). The turquoise lines summarize the gradient without radial mixing, the black lines show the resulting gradient profiles in the observable stellar populations.

As discussed above, the inside-out formation (top panel of Fig. 5) gives a strong positive contribution to the abundance gradient throughout the entire disc, which greatly weakens the gradient in the outer disc and even reverses the gradient at small galactocentric radius. Radial mixing, which is quite moderate in this model, tends to weaken the gradients, mostly by averaging between regions with large differences. The transition matrix in angular momentum, M , which describes the churning by giving the probability of having angular momentum L_z for a star with initial angular momentum $L_{z,0}$, will have larger off-diagonal terms for older stars, reflecting that the very metal-poor stars born at early times can migrate a bit further out than their metal-rich, younger counterparts. This effect is quite mild, if migration rates do not vary strongly with time, and if the angular momentum distribution is approximately conserved, in which case, the short disc scalelength limits outwards migration at very early times. The blurring term B has a straightforward effect on the gradient. We expect inner disc populations to be intrinsically hotter than their outer disc counterparts due to stronger heating, with another contribution from their older age. This means that inner disc populations get blurred towards larger radii. For MW-like set-ups, this should weaken any gradient inversion, but in particular, near cut-offs in the disc, it will play a dominant role. Interestingly, in the standard inside-out model, two separate effects counteract each other. On the one hand, radial mixing weakens the central metallicity peak, i.e. gives a positive gradient contribution, but it also pushes older and kinematically hotter inner disc stars further out, giving a negative gradient contribution. We also note that it is a well-known fact in chemical evolution modelling that inside-out formation strengthens the negative metallicity gradient in the star-forming ISM (Prantzos & Boissier 2000). Steep radial metallicity gradients far in excess of $-0.1 \text{ dex kpc}^{-1}$ have been observed in other galaxies (e.g. Jones et al. 2010, 2013).

The middle panel of Fig. 5 shows the inside-out model with additional mixing in the gas phase. This particularly flattens the gradient in the inner disc and reduces the contribution of the inherited gradient, while the star formation-related term stays nearly the same. As a result, the disc without radial mixing shows a very strong gradient inversion in the central region at $R < 5 \text{ kpc}$. This is ameliorated by radial mixing.

For contrast, the bottom panel of Fig. 5 shows the simulation with constant scalelength of the gas disc. Accordingly, the inner parts of the disc show no star formation contribution to the gradient, so only the averaged gradient and radial mixing play a role. In this case, the radial mixing contribution becomes significantly positive. The big negative excursion in the SFR related part around 12–15 kpc derives from the cut-off in the Schmidt–Kennicutt law, which very quickly

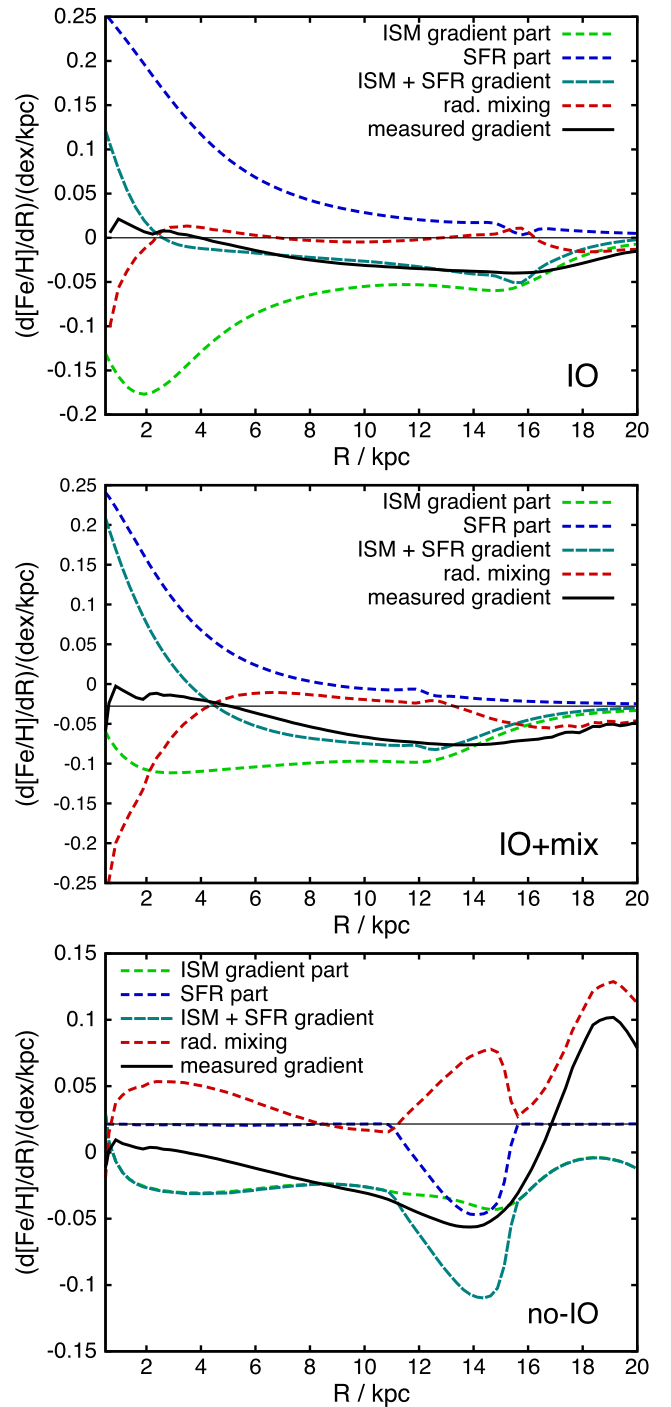


Figure 5. Metallicity gradients and their contributing parts in the standard simulation with inside-out formation (top), in the inside-out model with enhanced gas mixing (middle), and in the model with constant scalelength of the gas disc (bottom). The gradient without radial mixing is shown in dashed turquoise, split according to equation (18) into the star formation-averaged past gradient (green) and the contribution from the SFR changes (blue). The red dashed line shows the change of gradient by radial mixing, resulting in the final (observable) metallicity gradient (black solid line). Note that the model without inside-out formation still experiences a change in the cut-off radius, the dominant effect being a shrinking of the cut-off radius, when the accretion rates of the disc diminish. This leads to a negative contribution from the SFR term, somewhat compensated by the radial mixing of more metal-rich stars into the cut-off region.

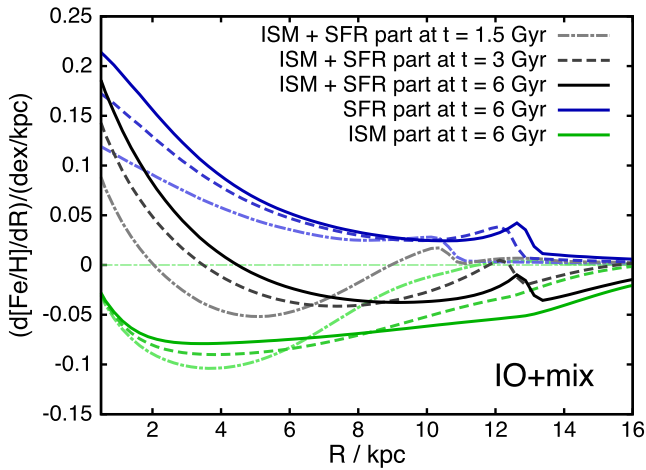


Figure 6. Time evolution of the ISM (green lines) and SFR (blue lines) contributions (first two terms of equation 18 in the model) with inside-out formation and enhanced gas mixing to the radial stellar metallicity gradient (black lines) without accounting for stellar radial mixing. Results are shown at $t = 1.5$ (dash-dotted lines), 3 (dashed) and 6 Gyr (solid lines).

expands to ~ 15 kpc after the start of the simulation, and then slowly travels inwards due to the declining accretion rates. Radial mixing partly compensates this by bringing in more metal-rich stars, and, in the outermost zone of this model, where densities vanish, even overcompensates due to the larger kinematic heat of inner disc stars.

In Fig. 6, we show the evolution of the impact of inside-out formation on stellar radial metallicity gradients (different line-types mark the different ages). We show in green the star formation-averaged radial metallicity gradient, while blue lines depict the inside-out contribution to $d[\text{Fe}/\text{H}]/dR$, and black lines show the resulting radial metallicity gradient in the stellar populations before accounting for stellar radial mixing. With our parameters, the impact of inside-out formation grows significantly in time up to an age of about 6 Gyr, which is mostly caused by the longer baseline of inside-out growth and the fact that the difference in the star formation histories g_* grows with time. Even at the earliest times or, respectively, at high redshift, the inside-out growth exerts a strong positive bias of the order of 0.1 dex kpc^{-1} , resulting in a mildly positive $d[\text{Fe}/\text{H}]/dR$.

4.1 Inside-out growth and observed stellar metallicity profiles

Fig. 7 compares radial metallicity profiles of the cold (star-forming) gas (left-hand column) and of the stars (centre and right-hand columns) at various different times in the simulation. The middle column shows the stellar metallicity profiles if we ignore any migration effects, and the right-hand column depicts the profile including the effects of typical blurring and churning over time. The main effects of the blurring and churning are an averaging between the metallicity gradients of neighbouring rings (see the factor T'_i in the first line of equation 17), to exert a negative bias on the radial metallicity gradient by moving the oldest (and more metal-poor) stars to larger radii, and with strong mixing to reduce (though not completely remove) radial gradients in the disc. The top row shows the results for our standard inside-out formation model (IO), the middle row shows that from the model with additional gas mixing (inside-out+MIX) and the bottom row shows the reference model without inside-out formation (no-inside-out).

Note, in particular, that in the inside-out models, at early times, the abundance profile in all components is steeper than in model no-inside-out. This is due to the shorter scalelength of the inner disc, the initially larger star formation efficiencies and the faster decline of the SFR in the central regions, which shifts the balance of yields to freshly accreted gas. However, while the simulation without inside-out formation shows persistently negative $d[\text{Fe}/\text{H}]/dR$ at all times, the inside-out formation models show a flattening of the (initially steeper) stellar abundance gradients with time, up to an inverted gradient in the central regions at later times.

The middle row shows our inside-out model with weakened radial metallicity gradient produced by strong radial mixing of both gas phases. This mixing is still counteracted by the inflow towards the disc centre, so a significant, albeit shallower gradient remains. It is not of interest to discuss if such a mixing is physical or not. Since there are many weakly constrained factors that influence abundance gradients in galaxies, we just use this one to achieve a weaker gradient without risking a gradient inversion within the star-forming gas. As a result, we see now that in the inner regions of the galaxy, the present abundance gradient in the stellar populations is dominated by the combined effect of rising metallicity with time and inside-out formation. The fact that more stars are formed at early times and lower metallicities becomes more important than the abundance gradient in the star-forming gas, which remains negative at all times. While radial migration again delivers a bias in the opposite direction, weakening the positive gradient, the inner regions still display the inverse gradient.

On a side note, we remark that inside-out growth very likely infers a negative $d[\alpha/\text{Fe}]/dR$ gradient. This has been noticed by Gibson et al. (2013). We would, however, like to discourage oxygen for these discussions: oxygen yields critically depend on the shell structure and hence, in particular, wind losses of massive stars (simply put, strong wind losses reduce the material available for helium burning), which, in turn, are related to metallicities (see e.g. early models from Maeder 1992). This is less critical for heavier alpha elements like magnesium. As an example, the $d[\text{O}/\text{Fe}]/dR$ gradient in SB09 was positive while any other alpha-to-iron element ratio in SB09 would be nearly flat in radius. Fig. 8 shows the radial profiles for the $[\text{Mg}/\text{Fe}]$ ratio. Some recent observations find the expected different trends in magnesium and oxygen (McWilliam et al. 2008; Genovali et al. 2015). The model without inside-out formation (red line) displays a very weak positive $d[\text{Mg}/\text{Fe}]/dR$, which is mostly caused by a very weak metallicity dependence of magnesium versus iron yields. Another contributing factor is the slightly outwards expansion by blurring, which is stronger for the oldest, alpha-rich populations. The stronger rise beyond the cut-off is again caused by the retraction of the cut-off with slowing infall. As expected, in the model with inside-out formation (blue line), the inside-out formation dominates over the other effects, leading to a negative $d[\text{Mg}/\text{Fe}]/dR$, again exacerbated at the cut-off. There are a couple of other complications preventing easy interpretations of observations: the inside-out formation leads to a central depression of the $[\alpha/\text{Fe}]$ values at intermediate to late times, which partially (and depending on the specific yield and flow models) compensates the inside-out effect. In addition, the exact behaviour depends also on the different re-distribution of SNIa yields compared to SNIi yields, loss rates and inflow abundances.

To summarize, we have shown that if inside-out evolution has a comparable time-scale to the enrichment time-scale in a galaxy, the stellar populations are liable to acquire an inverse (positive) radial gradient, even if the radial metallicity gradient in the star-forming gas is negative at all times.

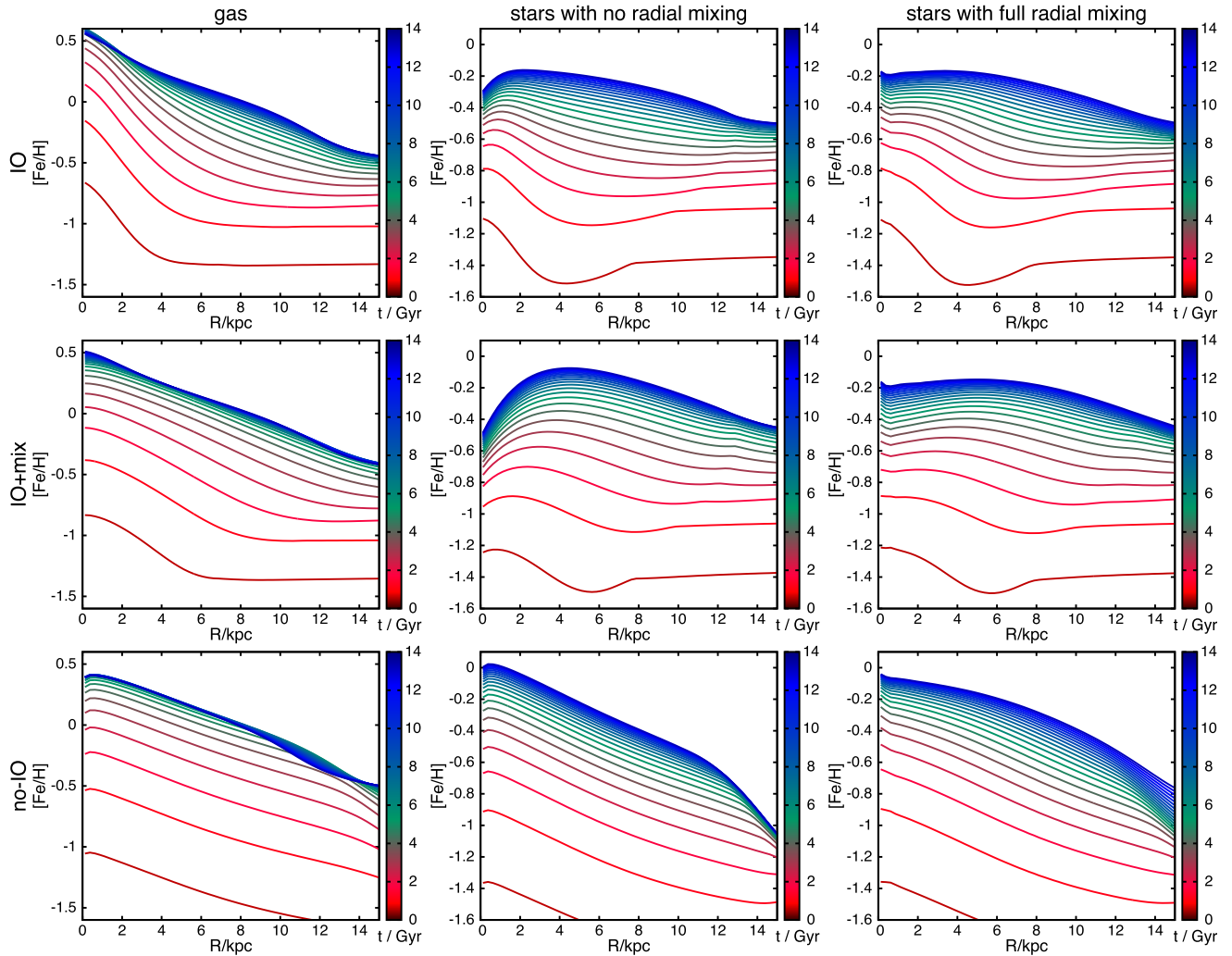


Figure 7. Left-hand column: metallicity profiles in the star-forming gas at different times in the simulation (colour coded). We show the same models as before, i.e. the ‘standard’ inside-out model on top, the inside-out model with additional gas mixing in the centre and the model with constant scalelength in the bottom row. The centre column shows each model the average metallicity of stellar populations without accounting for radial mixing, while the right-hand column accounts for radial mixing.

4.2 A source of inverse/positive metallicity gradients in the cold gas: re-distribution

We have shown in the previous sections that inverse gradients in the stellar populations are a natural consequence of inside-out formation. However, it is still important to discuss the possibility of inverse gradients in the star-forming gas itself. So far, the two main explanations invoked for this possibility have been a direct accretion of cold metal-poor gas into the central regions (Cresci et al. 2010) and the rather peculiar chemical evolution argument of Curir et al. (2012). In the first case, it is unclear how accretion of metal-poor material would manage to pierce into the centre in a sufficient amount to offset the higher star formation efficiencies and prevent an inward flow through the disc (both of which drive a negative radial metallicity gradient). The second case (Curir et al. 2012) produces a very small signal, and, while an intriguing idea, also depends on the specific and arbitrary changes in the star formation efficiencies applied in their underlying chemical evolution models. It can be shown analytically, and we have also confirmed in tests that our chemical evolution model in its standard set-up does not produce any gradient inversion in the star-forming gas when we remove radial flows

and mixing from our model to match the classical evolution models of Spitoni & Matteucci (2011) and Curir et al. (2012), unless we impose significantly higher loss rates in the central regions (which is a different argument).

However, the radial re-distribution of metals within the galaxy does open a viable path to creating inverse gradients in the star-forming gas. Only a fraction of the stellar yields will be directly recycled to the cold star-forming gas phase (the direct enrichment parameter in our model), while half the yields or more end up in the warm and hot ISM, a part of them being expelled from the galaxy, a part of them lingering near the disc. The unhappy truth is that we know nearly nothing about this re-distribution, apart from some information on the rotation of the coronal gas (see e.g. Marinacci et al. 2011; Marasco, Fraternali & Binney 2012). The angular momentum difference with the disc might not only drive inflow in the disc, but angular momentum and pressure from stellar yields might push, in turn, the coronal gas outwards. This can result in the enriched, hot material condensing back on to the disc at larger radii than its production. If this effect is strong enough, it can invert the metallicity gradient in the star-forming gas.

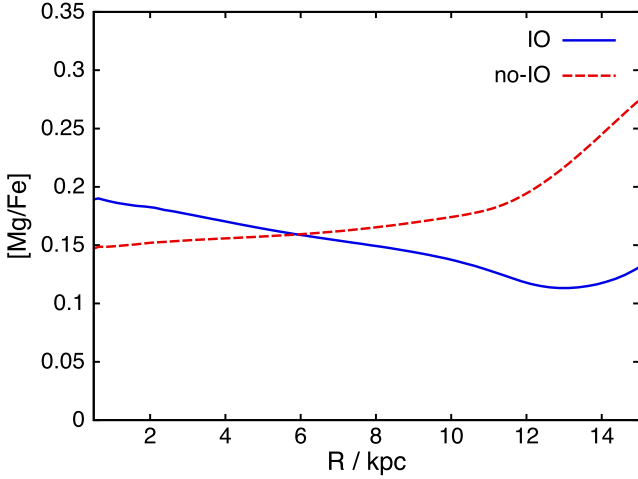


Figure 8. Stellar $[\text{Mg}/\text{Fe}]$ profiles of the standard model with inside-out formation (blue) and the model without inside-out formation (red).

We can identify three natural processes that would yield an early gradient inversion.

- (i) Re-distribution of the yields near the disc as detailed above.
- (ii) Loss of material/yields: The intense star formation of the central regions and potentially activity of the central black hole will drive a stronger outflow. Outflow from the central regions of disc galaxies (usually perpendicular to the disc plane) has been observed; for the MW, see Bland-Hawthorn & Cohen (2003), and for M82, see Shoppell & Bland-Hawthorn (1998). It is natural to assume a higher loss rate for yields from central regions in particular at early times when the SFRs are higher and more concentrated.
- (iii) Re-accretion of enriched material: Little is known about the spatial distribution of yields from galaxies near the boundary to the IGM. It can be assumed though that a fraction of the enriched outflow mixes with the infalling material especially at high redshifts. If the time-scale of re-accretion is shorter than the star formation time-scale of the disc, the (re-accreted) material can quite easily obtain higher metallicities than the gas disc. Two factors help here: Due to the inflow through the disc, the outer disc will have more recently accreted material, i.e. an increasing metallicity of the accreted ISM contributes to an inverted metallicity gradient. More importantly, the inside-out formation of the disc demands that in relation to the present mass, more fresh material is accreted on to the outskirts.

Fig. 9 shows an example of gradient inversion by a galactic fountain. As a parameter change from the standard model, we increase the fraction of lost material to 80 per cent in the outer regions and 90 per cent in the innermost 4 kpc. Instead of pre-setting the metallicity of the freshly accreted gas, we assume that one quarter of the lost gas is re-accreted, mixing with primordial gas, up to a maximum metallicity for the infalling gas of $[\text{Fe}/\text{H}] = -0.7$. It can be seen that during the first ~ 0.6 Gyr, the radial metallicity gradient is inverted, due to the re-accretion of material at higher metallicities than the young disc. This inversion could last significantly longer and to higher metallicities with a more metal-rich inflow, as the re-accretion fraction might be higher, and we do not see an a priori restriction on the upper bound to the inflow metallicity. At later times, the gradient normalizes. As pointed out above, this is just one of many natural factors that favour inverse metallicity gradients in young discs and do not require any cold streams piercing into the central galaxy.

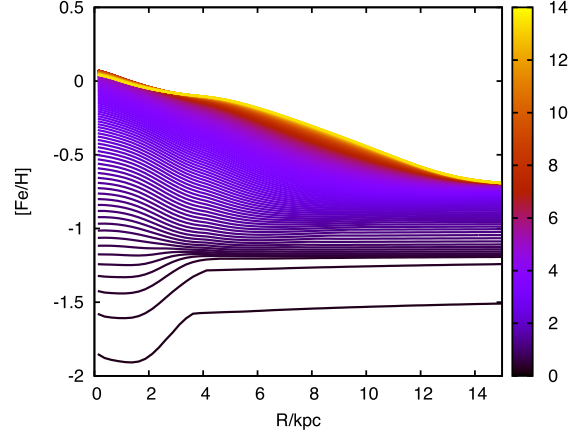


Figure 9. Metallicity profiles in the star-forming gas for an alternate model with higher loss rates and re-accretion of one quarter of the lost material with the infall of fresh gas. With the inside-out growth, a lot of material is present in the inner rings, while the outer rings (beyond ~ 4 kpc) experience quite rapid accretion of relatively more enriched material. This results in a gradient inversion of this model in the first ~ 600 Myr. The model is plotted every 75 Myr for the first Gyr and then at the multiples of 0.75 Gyr.

4.3 Relation to simple chemical evolution models

Classical chemical evolution models have failed to predict gradient inversions in the stellar populations under inside-out formation, while discussing in great detail the steepening effects of inside-out formation on the star-forming ISM (Prantzos & Boissier 2000). At least, a part of the cause is that the classical evolution assumptions lead to an unnaturally strong coupling between star formation and enrichment rates. This is primarily due to the one-phase treatment of the gas and missing radial exchange, and in some cases, the assumption of instantaneous recycling. Many chemical evolution models assume that star formation cycles can be broken down into infinitesimally short time bins, in which each infinitesimally small star formation cohort enriches the gas for its successors immediately (an assumption that is still frequently taken for SNII yields). Under those assumptions, the metallicity in the ISM would be mostly a function of the present stellar mass. To give a simple example: the simple accreting box model has a metallicity of

$$Z_b(t) = p \cdot \left(1 - \exp \left(1 - \frac{M_s(t)}{M_g} \right) \right), \quad (19)$$

where p and $M_s(t)$ are stellar yields and the stellar mass at time t , while M_g is the (constant) gas mass. This model is sufficiently simple, such that we can write the equivalent of equation (6) as

$$\langle Z \rangle = \frac{1}{M_{s,\text{final}}} \int_0^{t_{\text{final}}} Z_b(t) \frac{dM_s(t)}{dt} dt. \quad (20)$$

As Z_b does not depend explicitly on t , but only on $M_s(t)$

$$\langle Z \rangle = \frac{1}{M_{s,\text{final}}} \int_0^{M_{s,\text{final}}} Z_b(M_s) dM_s. \quad (21)$$

Therefore, the final mean metallicity at each $L_{z,0}$ is independent of the details of the star formation history, and only depends on the total star formation in the given radial bin. As a result, this simple model (wrongly) predicts that inside-out formation leaves the stellar radial metallicity gradient nearly unaffected.

To test this with our models, several parameters have to be changed to approximate a simplified chemical evolution code. We set the fraction of yields going to the warm/hot ISM to 0.005, and freeze out 0.99 of this per time-step. Also, we free all yields from

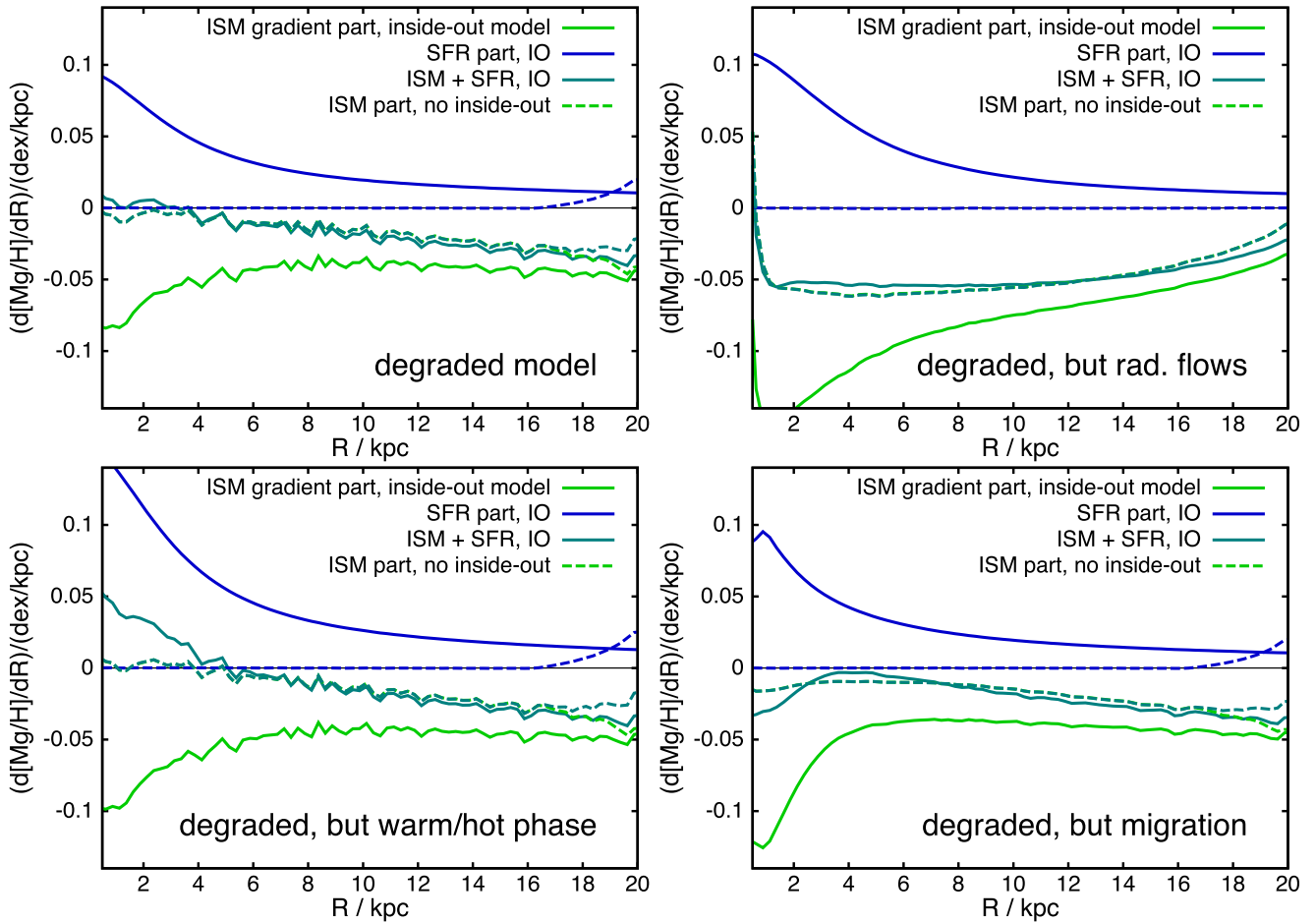


Figure 10. The top left-hand plot shows $d[Mg/H]/dR$ profiles for simplified models with near-instantaneous enrichment, no hot gas phase and no migration. Dashed lines are the model without inside-out formation, solid lines show its inside-out formation counterpart. As in Fig. 5, the resulting gradient profile (without migration) in the stellar populations is painted in turquoise. Its contributions from the time-averaged metallicity gradient and from the changing star formation history with radius are painted in green and blue. In the other three panels, we selectively re-instate one of our more realistic approximations for either radial flows (top right), a warm/hot phase (bottom left) and radial mixing in the gas and stars (bottom right).

the first 7.5 Gyr in the first time-step, set the SNIa delay time to 15 Myr and evaluate magnesium instead of iron. Further, we set the inflow composition to primordial, eliminate radial flows by setting the specific angular momentum of the infalling gas to that of a circular orbit at each radius, eliminate gas mixing and switch off churning, by setting the migration parameter to 10^{-6} . With this degraded model, the top left-hand panel of Fig. 10 analyses the standard inside-out formation history (solid lines) in comparison with a constant scalelength model with gas disc scalelength of 3.25 kpc (dashed lines). The colours are chosen to match Fig. 5; however, since radial mixing is switched off, only the first terms of equation (17) are of interest. As expected, the inside-out model has a far steeper star formation-averaged gradient (green solid line) than its constant scalelength counterpart. However, this steeper gradient is almost fully compensated by the gradient contribution from the radially dependent star formation history (the contribution is near-zero for the model with constant scalelength). As a result, the observable metallicity gradient in today's stellar populations is almost exactly the same in both cases. Minor differences arise mostly from the finite time resolution of the model, which sets a minimum delay time for the stellar yields at the time resolution of 15 Myr and has some importance at the lowest metallicities, in particular, in the intensely star-forming inner regions. Further, the star for-

mation histories and gradients will not perfectly match up due to different degrees of saturation (in the outer rings, the ratio between stellar mass and present gas is low, and hence metallicity has yet to approach its equilibrium value). The other three panels of Fig. 10 show the effects of switching back on single aspects of our full model. As can be expected, the presence of a warm-hot gas phase mostly affects the quick changes in the inner regions, giving a very large positive effect on the gradient in the inner regions. The redistribution via migration has a tendency to move metals outwards and hence contributes negatively in the innermost regions and positively at inner to intermediate radii. Radial flows create the general abundance gradient, but have only minor effects on behavioural differences between inside-out and constant scalelength models. This is reasonable, since the gas flows only a relatively short distance during a typical enrichment time, so that flows do not connect vastly different regimes.

This comparison conveys two important messages: the detailed star formation history has to remain strictly coupled to chemical evolution, otherwise the mismatch between enrichment and SFRs will alter the metallicity gradients. While useful for other problems, 'painted' N -body models with separately calculated, more sophisticated chemical evolution (Curir et al. 2012) should not be used for assessing radial metallicity gradients or relationships between

chemistry and kinematics, unless they exactly preserve the same star formation history in both the N -body and chemical evolution part. This is particularly the case for combinations that have large discrepancies between the early star formation in their chemical evolution models versus the N -body part (see fig. A.1 in Minchev et al. 2014).

More importantly, this demonstrates the importance of radial flows, mixing and processes that delay enrichment in young galaxies. These processes greatly alter the observed metallicity gradient: (i) radial mixing flattens the ISM gradients, while radial inflow tends to steepen them. (ii) The metallicity of the inflowing gas will change with time as the enrichment of the IGM proceeds, (iii) metals get locked up in the warm and hot ISM of a galaxy, from which they only freeze out with a significant time delay, and (iv) the time between the initial collapse of a molecular cloud and the first yields is of the order of 10 Myr. No matter the assumptions, any star formation spike on a time-scale shorter than this will (apart from direct enrichment from neighbouring supernovae) be dominantly influenced just by the preceding metallicity of the ISM. Points (i), (iii) and (iv) are the main factors driving inverted gradients in stellar populations, but most chemical evolution models neglect at least some of them.

5 KINEMATIC GRADIENTS

Gradients in mean azimuthal speed depending on metallicity as first found by Spagna et al. (2010) have to be explained by two different factors: asymmetric drift by kinematic heat of each metallicity cohort and their angular momentum distributions, both factors determining the local asymmetric drift. Following the example of equation (5), we can write

$$\langle V_\phi(Z_x, R) \rangle = W_f^{-1} \iint \frac{L_z}{R} s_{Z_b=Z_x} g_\star(L_z, t) M(L_{z,0}, L_z, t) \times B(L_z, R, t) dt dL_z dL_{z,0}, \quad (22)$$

where $s_{Z_b \in Z_x}$ selects populations only when Z_b is in the interval Z_x , and W_f is a normalization:

$$W_f = \iint s_{Z_b \in Z_x} g_\star(L_z, t) M(L_{z,0}, L_z, t) B(L_z, R, t) dt dL_z dL_{z,0}. \quad (23)$$

It can be directly seen that while structurally similar, this has a different behaviour from equation (18). In contrast to the mean metallicity, the factor L_z prevents us from merging the churning and blurring terms. If we take the bin Z_x to be infinitesimally narrow, and if we assume that the metallicity rises monotonically, the object $s_{Z_b=Z_x}$ will pick the populations at the point when the metallicity of Z_x is reached with a weight inversely proportional to $\partial_t Z(L_{z,0}, t)$, i.e. to the rate of change of the metallicity at that time. This raises again the important point about delayed enrichment. In the overly simple model from Section 4.3, a faster SFR just speeds up enrichment roughly proportionally, which implies that the changes in g_\star and the evolution of Z cancel out in this equation. This does not happen in a model that incorporates delayed enrichment and chemical evolution.

Fig. 11 shows the mean azimuthal velocities at each metallicity bin in the inside-out model (coloured) versus the same quantities in a model with constant scalelength ($R_{d,gas} = 3.5$ kpc) of the gas disc (green points). It is apparent that while the metallicity gradients have similar values in both cases, the scalelength growth produces a strong dependence between mean azimuthal velocity and metallicity. To create this plot, we calculated the abundance

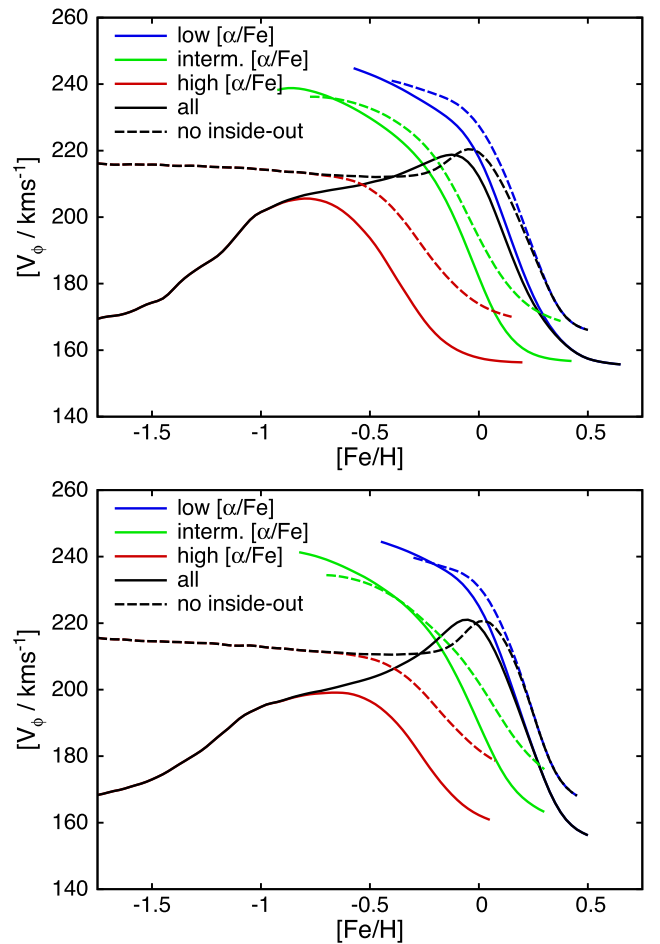


Figure 11. Mean azimuthal velocity at each metallicity bin in the inside-out model (black lines), and the mean V_ϕ in the $[\alpha/\text{Fe}]$ bins with delimiters $-0.05, 0.10, 0.25$ dex (colours). To make a more ‘realistic’ case, for this plot and all subsequent V_ϕ versus $[\text{Fe}/\text{H}]$ statistics, we sum all stellar populations (mass-weighted) in the model in the altitude range $0.4 \text{ kpc} < z < 0.8 \text{ kpc}$ and fold the abundance determinations with optimistic Gaussian errors of $\sigma = 0.05$ dex both in $[\text{Fe}/\text{H}]$ and in $[\alpha/\text{Fe}]$. The top panel shows the ‘standard’ inside-out model (solid lines) compared to a model with constant gas disc scalelength (dashed lines) of 3.5 kpc (i.e. no inside-out formation at all). The bottom panel shows the same constant scalelength model, but the inside-out model with strong gas mixing and hence reduced radial metallicity gradient.

plane at $R = 8 \text{ kpc}$ integrating over $0.4 \text{ kpc} < z < 0.8 \text{ kpc}$, folded it with a Gaussian observational error in $[\alpha/\text{Fe}]$ and $[\text{Fe}/\text{H}]$, and evaluated the mean azimuthal velocity versus metallicity for the entire sample (yellow points) and for different $[\alpha/\text{Fe}]$ bins with delimiters at $[\alpha/\text{Fe}] = -0.05, 0.10, 0.25$ dex. The behaviour can be quite easily explained. The youngest stars with largest azimuthal velocities dominate the two lower $[\alpha/\text{Fe}]$ bins. For them, the recent/current abundance gradient of the galactic disc dominates the velocity structure. While radial migration with the SB09 coefficients induces strong mixing in angular momentum of stars, enabling us to see large numbers of stars with different metallicities, the migration is not complete, i.e. low-metallicity stars are still preferentially located at larger guiding centre radii than their metal-rich counterparts. Together with mildly reduced velocity dispersions for the metal-poor stars (they are outer disc populations), those metal-poor low-alpha stars can even reach mean azimuthal velocities above the local circular speed (this observation was discussed e.g. by

Haywood 2008), while the metal-rich stars still concentrated in the inner regions attain low azimuthal velocities. For an in-depth discussion of Strömberg's equation governing this behaviour, see Schönrich, Binney & Dehnen (2010).

A very important characteristic of these kinematics is the slope of $dV_\phi/d[\text{Fe}/\text{H}]$ at the metal-rich rim of the high $[\alpha/\text{Fe}]$ population. This is very difficult to assess in current surveys because of the decreasing number of high $[\alpha/\text{Fe}]$ stars with increasing $[\text{Fe}/\text{H}]$. Hence, the fraction of low $[\alpha/\text{Fe}]$ stars at the same metallicity increases, so that increasing contamination with higher V_ϕ populations is a major issue (in this light, it is also unwise to use a sample selection sloping in $[\alpha/\text{Fe}]$ versus $[\text{Fe}/\text{H}]$). However, if the structure of this branch can be determined, it gives direct insight into the situation of the old disc, when significant SNIa enrichment sets in. If there was a significant radial metallicity gradient in the disc at that time, the trajectories of the outer regions of this disc will have their $[\alpha/\text{Fe}]$ versus $[\text{Fe}/\text{H}]$ knee at a lower $[\text{Fe}/\text{H}]$ than their inner disc counterparts. While all environments run through the same high $[\alpha/\text{Fe}]$ -low $[\text{Fe}/\text{H}]$ points, the metal-rich end of this sequence will hence show some differentiation. In the presence of negative $d[\text{Fe}/\text{H}]/dR$, only the innermost radii can still contribute to the highest metallicity bins, implying negative $dV_\phi/d[\text{Fe}/\text{H}]$. If the ISM gradient at this time was indeed inverted/positive, the age-dispersion relation would compete with a positive correlation from the radial gradient, which could be resolved by comparing velocity dispersions and the asymmetric drift.

Fig. 12 explores the parameter space for the inside-out growth of the disc. The top panel shows the mean azimuthal velocity as in Fig. 11 for different initial scalelengths $R_{g,0}$ of the gas disc (cf. equation 1). We need substantial inside-out growth to achieve a reasonable effect on $dV_\phi/d[\text{Fe}/\text{H}]$. The effect is nearly proportional to the amount of disc growth, which is evident, since the current disc scalelength translates directly into asymmetric drift, and churning does little to change the distribution. We also note that the mild bump in the velocity–metallicity relations for the entire disc around $[\text{Fe}/\text{H}] \sim -1$ is partly caused by a strong early slowdown in the increase of the infall metallicity, and would be entirely removed, if the cut-off of the early disc would be at smaller radii or if the infall metallicity had a more linear time-dependence. We tested that it does not affect the general behaviour of our models beyond this bump.

The time-scale of disc growth is limited by the bottom panel of Fig. 12. If the disc evolves too fast, there will be no effect; if the growth is too slow, the disc will have the major part of its evolution after the high $[\alpha/\text{Fe}]$ stars have branched off. For example, in the model with the longest inside-out formation time-scale of 5 Gyr, the branching point for the high $[\alpha/\text{Fe}]$ stars lies only around $V_\phi \sim 170 \text{ km s}^{-1}$.

Note that there is a shift in the mean metallicity in particular of the outer regions. This is because we keep all other parameters fixed, i.e. we use the same time-dependent accretion rates for all models, which results in significant differences between models in today's stellar mass profiles and hence enrichment.

5.1 Kinematic heat and blurring

Fig. 13 shows the changes experienced by the two gradients when we change the heating law in our galaxy. For this purpose, we exchange the standard heating law that is a space-dependent $\tau^{0.33}$ power law in age, with a 'broken' thin-thick disc law. For this purpose, we keep the $\tau^{0.33}$ power law up to age 10 Gyr, but scale all velocity dispersions down by a factor of 1.5, and then set a linear

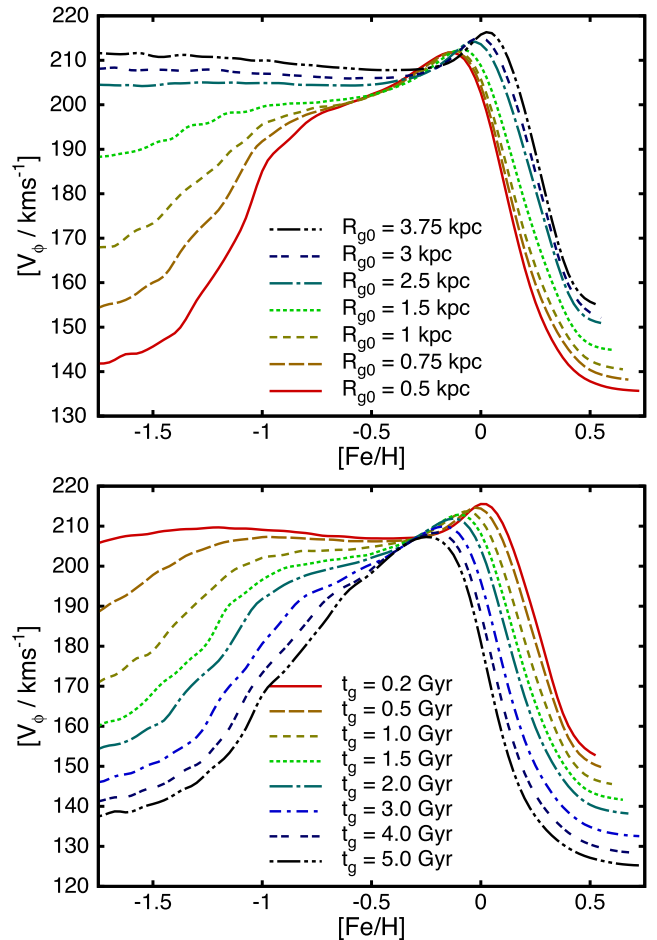


Figure 12. Varying the parameters on the inside-out formation. The top panel shows the mean azimuthal velocity versus metallicity as in Fig. (11) for different initial scalelengths of the gas disc at a growth time-scale of $t_g = 2$ Gyr. The bottom panel shows the same relation for an initial scalelength of the gas disc of $R_{g,0} = 0.75$ kpc, but different growth rates t_g .

rise to double the dispersion between 10 and 11.5 Gyr, keeping the dispersion flat afterwards. This distribution resembles somewhat the broken time-dependence in Sanders & Binney (2015) and looks also similar to 'upside-down' galaxy simulations (Bird et al. 2013). As we discussed before, this affects the statistics in $dV_\phi/d[\text{Fe}/\text{H}]$ and $d[\text{Fe}/\text{H}]/dR$ in opposite ways. The spreading of the oldest stars makes the gradient more negative throughout the disc and essentially eliminates the region with inverse/positive gradient. However, this implies a larger asymmetric drift for the most metal-poor stars, which increases the gradient of rotational speed with metallicity for thick disc stars. While the general structure is unchanged, there is a significant decrease in the $dV_\phi/d[\text{Fe}/\text{H}]$ slope at the high-metallicity end of the high $[\alpha/\text{Fe}]$ subgroup, essentially rendering the trajectory flat. While population densities are extremely low down this tail, this could be an interesting diagnostic in large data samples. From the constant scalelength model, we can see that the effect on the azimuthal velocities is of the order of 20 km s^{-1} , which is already comparable to the effects observed in local samples. The take-away message is that while the gradient for the thick disc points to an inside-out formation, the exact quantification has to await more precise constraints for the heating law and metallicity data throughout the disc, since the blurring effect has an inverse sign to the inside-out formation impact on gradients.

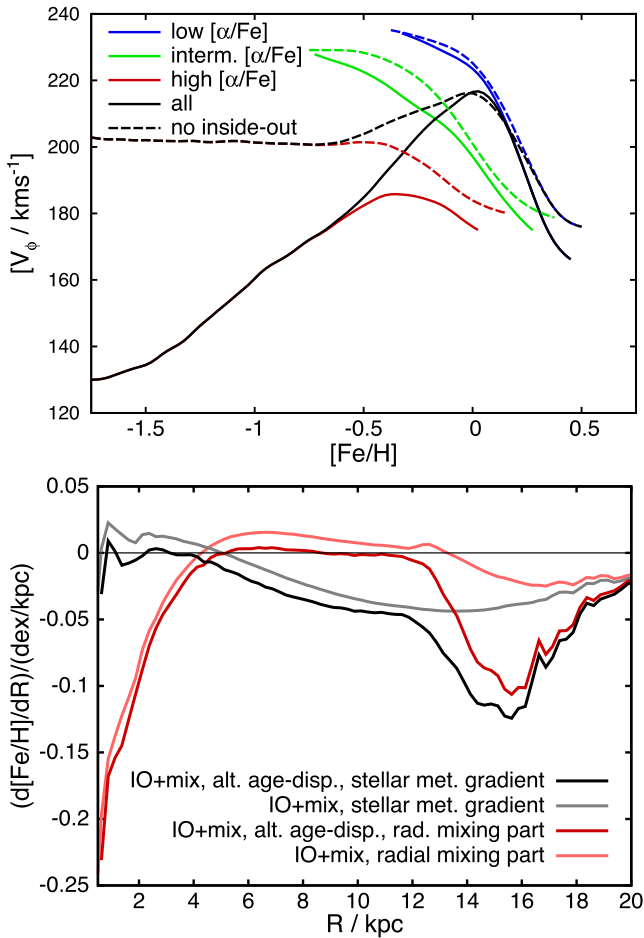


Figure 13. Top panel: V_ϕ versus $[\text{Fe}/\text{H}]$ profiles (black lines) as in Fig. (11) for the standard inside out (inside-out, solid lines) and constant scalelength models (no-inside-out, dashed), but with the altered age–dispersion relation. Coloured lines show $[\alpha/\text{Fe}]$ bins with delimiters $-0.05, 0.10, 0.25$ dex as in Fig. 11. Bottom panel: observable radial metallicity gradient profile in the stellar populations and its radial mixing contribution for the model with altered age–velocity relation compared to the inside-out model with strong gas mixing.

6 GRADIENTS OFF THE PLANE

Lastly, we look into the effect on gradients in and above the disc plane. It is a priori clear that with these assumptions, models with inside-out formation should display a steeper negative vertical metallicity gradient than constant scalelength models. This is because inside-out formation produces more low-metallicity stars with hot kinematics, and in particular, a larger number of low-metallicity stars in the innermost regions (which we believe to be kinematically hotter) than in the outer disc regions. This is mediated by the transition term T in equation (6). Towards higher altitudes, the fraction of older stars generally increases, but at larger radii, the younger populations can still contribute more stars because some are radially migrated outwards, bringing more intermediate-age/younger ages to larger altitudes at intermediate to large galactocentric radii, due to the increasing scaleheight in outwards migration. That is, radial migration typically gives a positive trend towards $d[\text{Fe}/\text{H}]/dz$. This mixture of different ages is fully in line with observations. Casagrande et al. (2016) find a major contribution from stars at intermediate ages out to $z \sim 1$ kpc. Their gradient of the mean age of stars with altitude, $d\tau/dz = (4 \pm 2) \text{ Gyr kpc}^{-1}$, is quite ex-

actly in line with our model, which ages from a mean of 5 Gyr at $z \sim 0.05$ kpc to a mean age of 9 Gyr at $z = 1$ kpc.

Fig. 14 shows the corresponding metallicity profiles. In the two models with radial mixing (top row), the inversion point of the radial metallicity gradient shifts to successively larger radii towards larger altitudes. In addition, the inside-out formation (left-hand column versus constant scalelength models on the right-hand column) clearly enhances the vertical metallicity gradient at inner and intermediate radii, just because more metal-poor kinematically hot stars are present. This pushes the gradients also into the range of estimates from Kordopatis et al. (2011) and Schlesinger et al. (2014), with the same structure as noted in Schlesinger et al. (2014) that the decrease in metallicity is largely associated with the dominance of high $[\alpha/\text{Fe}]$ over low $[\alpha/\text{Fe}]$ stars.

Comparing the no-churning model to the inside-out model with churning, we see the same effect as noted in Kawata et al. (2017): For a disc with a near-constant initial scaleheight (as set in our model) stars from the inner disc have larger vertical actions and attain larger scaleheights, which can give a positive contribution to $d[\text{Fe}/\text{H}]/dz$. However, as noted above, the vertical gradient depends critically on the enrichment history of the disc. Due to large age uncertainties, this is even true when attempting to select a single age group. The age–metallicity relation will generally give a negative contribution to the vertical metallicity gradient, while the weakening of radial gradients by inside-out formation makes the inner disc stellar populations more metal-poor and thus again negatively contributes to $d[\text{Fe}/\text{H}]/dz$.

The effect near the disc cut-off is also very interesting. The cut-off is a dominant factor in inverting the vertical metallicity structure of the disc. Because the immigrated objects have a stronger impact than the local populations, the structure is mostly determined by the rates of immigration from different radii, and we lose the always negative contribution to $d[\text{Fe}/\text{H}]/dz$ from the local populations. In the model without inside-out formation, the more metal-rich populations from further inside dominate the effect, while, in contrast, the inside-out models get a strong negative contribution from the large number of metal-poor stars reaching larger z . The trend towards very low metallicities at the lower altitudes of the model without inside-out formation stems from the contraction of the cut-off radius with the slowing infall, which, in this model, makes the vast majority of the kinematically cold, locally formed populations beyond the cut-off, old and metal-poor. We also warn that the heating assumptions here cast a bias, mostly carried by intrinsic outer disc populations migrating inwards. Since those would experience the higher heating rates in the inner regions, our assumption underestimates their dispersions and holds them too close to the plane.

To complete this discussion, Fig. 15 shows two alternative versions of the standard model. The top panel shows the inside-out model with additional mixing. As can be expected from our prior discussions on radial metallicity gradients for the entire disc, the main difference to the ‘standard’ inside-out model is moving the gradient inversion point to larger radii, while the general behaviour with altitude is very similar.

The bottom panel of Fig. 15 shows the same model with the ‘broken’ thin–thick disc heating law. Due to the disproportionately increased vertical velocity dispersions for the oldest and most populations, this model displays vertical metallicity gradients that are at the upper end of what may still be compatible with observations, indicating that the vertical metallicity gradient alone could serve to rule out the most extreme models in both galactic and extragalactic data. The drastic decrease in velocity dispersion over short time-scales, while the alpha-rich population is forming, is responsible

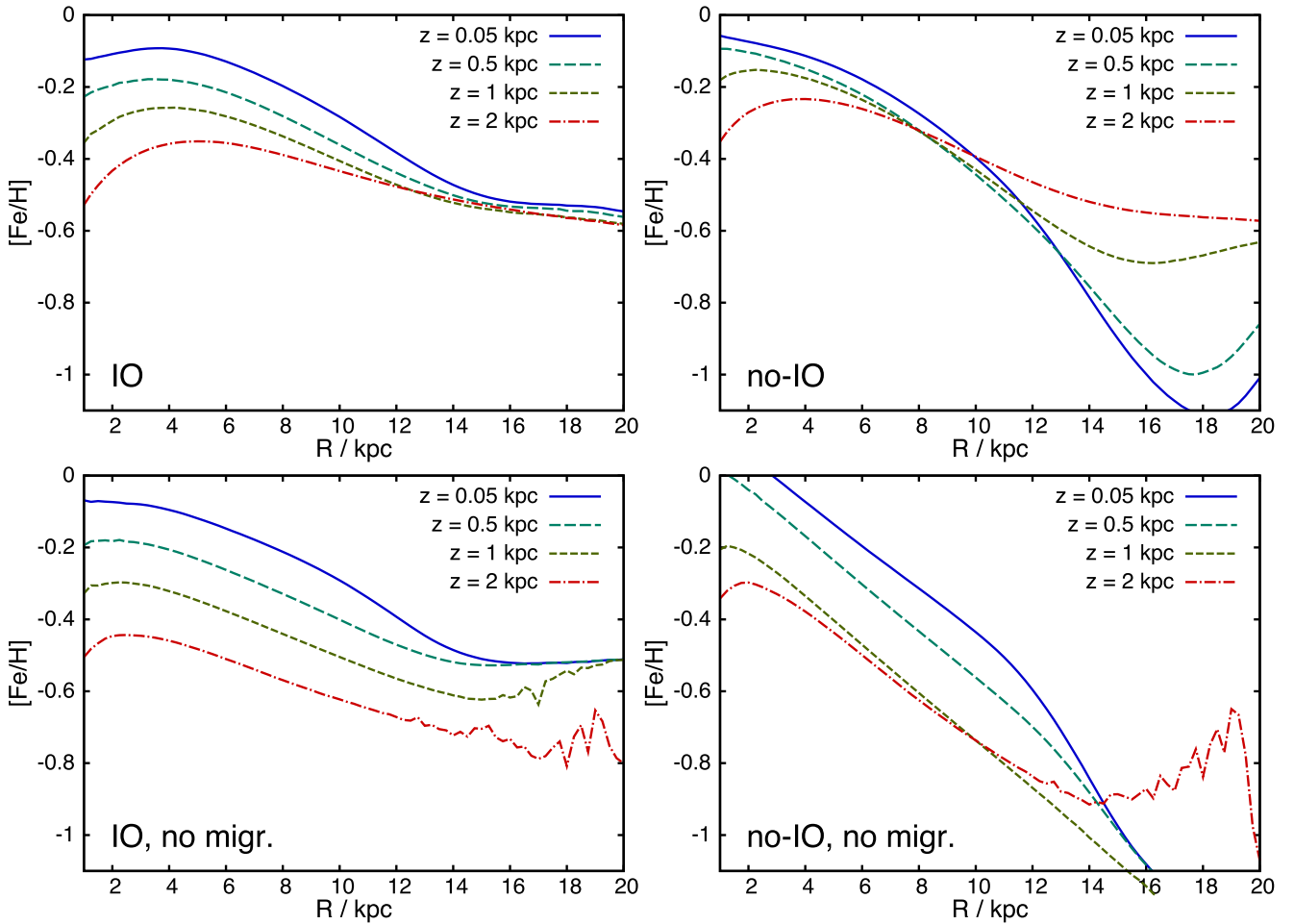


Figure 14. Metallicity profiles at different altitudes versus radius. The flattening and partly inversion of radial metallicity gradients is apparent in all models. The top left-hand panel shows the standard inside-out model. The four panels are arranged in a matrix with inside-out models on the left versus constant scalelength on the right-hand side, while models with radial migration are in the top row and models without churning are in the bottom row. While inside-out formation generally gives a positive contribution to the radial metallicity gradient, the dominant term behind the trend with altitude above the plane is radial re-distribution of the stars (churning).

for the particular steepening beyond $z > 1$ kpc. Also, this enhances the gradient inversion towards higher altitudes in the inner regions, and the steep radial metallicity gradients at large altitudes will be a major constraint for this type of models in the upcoming data sets.

To summarize, inside-out formation leads to a significantly more negative vertical metallicity gradient throughout the inner and intermediate disc regions. Gradient flattening and gradient inversions towards higher altitudes should not be ascribed to inside-out formation or radial migration alone, but both factors are synergetic. Thin–thick disc-like changes in the dispersions are particularly important to make outer disc vertical metallicity gradients more negative, but we caution that a similar effect can be achieved by stronger inside-out formation, and if the inner disc star formation dies out quite quickly (within a time-scale of ~ 2 Gyr).

7 CONCLUSIONS

In this paper, we have shown that when interpreting metallicity distributions of stellar populations, the full star formation history of the system has to be taken into account. We have demonstrated that radial metallicity gradients $d[\text{Fe}/\text{H}]/dR$ cannot be naively linked the metallicity gradients in the star-forming ISM. Instead, as we

differentiate in equation (18), the observed radial metallicity gradient in stars in a typical galactic disc is determined by three nearly equipollent factors: (i) the averaged radial gradient of the star-forming ISM, (ii) the inside-out formation of the disc and (iii) radial mixing in the stellar populations. Typically, we expect the inside-out formation of a disc to take place on a comparable time-scale to its initial enrichment (by typically $\gtrsim 1$ dex within the first ~ 2 Gyr). Consequently, the inside-out formation easily makes a positive contribution of $\gtrsim 0.1$ dex kpc^{-1} to the observed stellar metallicity gradient, and can result in a positive/inverted radial metallicity gradient. Thus, findings of inverse metallicity gradients in extragalactic observations are not a surprise, but a natural consequence of the inside-out formation. As seen in equation (18), the radial mixing of stars to first order averages the metallicity gradients from different radii. Strong radial mixing contributes to a flattening of gradients, and the larger velocity dispersions of older and more metal-poor stellar populations contribute a moderately negative term to $d[\text{Fe}/\text{H}]/dR$.

The observed signatures (stellar metallicity gradients, velocity–metallicity correlations) critically depend on the exact relationship between SFRs and chemical enrichment. In particular, in a simple chemical evolution model without delayed enrichment, without hot gas phase and without radial migration and flows, inside-out

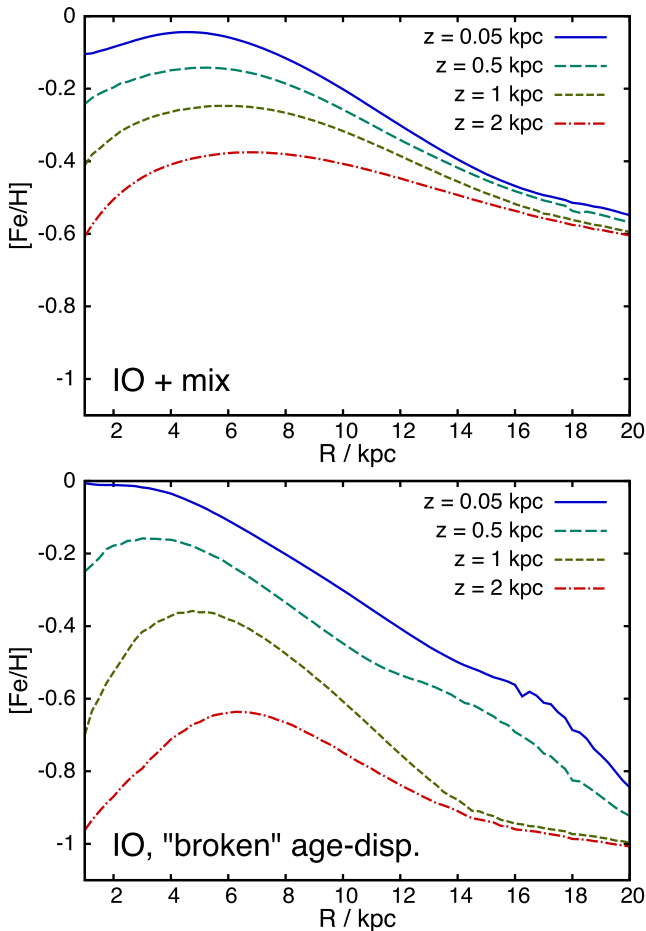


Figure 15. Metallicity profiles at different altitudes versus radius in two alternative versions of the model. The top panel shows the ‘standard model’ with additional gas mixing. The bottom panel shows the standard inside-out model, but with a ‘broken’ thin-thick disc heating prescription, reducing the velocity dispersions of thin disc stars, while increasing them strongly for the oldest populations.

formation has nearly no effect on today’s stellar metallicity gradients, since the faster enrichment compensates the larger number of stars formed in the inner galaxy early on. As seen in Fig. 10, the storage of yields in a hot non-star forming phase is primarily responsible for the strong impact of the inside-out formation on the observed metallicity gradient, especially in the inner regions. This process (and the re-distribution of the yields by lateral exchange, which has a smaller but non-negligible effect) decouples enrichment from the SFRs on short time-scales. This also implies that e.g. N -body models painted with a sophisticated chemical evolution should not be used to infer radial abundance gradients and chemo-kinematic relationships, as long as they cannot perfectly match the SFRs and radial flows between their N -body and chemical evolution parts.

We have further discussed the finding in the Milky Way of an inverse relationship of mean azimuthal speed versus metallicity for (thick) disc stars (Spagna et al. 2010; Lee et al. 2011). Just as in the question of inverse gradients, these inverse relationships are, by no means, an indication of inverted radial metallicity gradients of the past star forming ISM, but instead are fully explained by the inside-out formation of the Milky Way disc. Turning this argument around, they provide strong evidence for an early inside-out formation of the Milky Way disc that took place on the same time-scale,

~ 2 Gyr, as thick disc formation and SNIa enrichment. Our simple model also reproduces and explains the general structure of the observations: negative $dV_\phi/d[\text{Fe}/\text{H}]$ at relatively large V_ϕ for the low $[\alpha/\text{Fe}]$ populations is caused by the metallicity gradient of the disc, altered by radial migration/churning. The latter is responsible for the relatively small value of $|dV_\phi/d[\text{Fe}/\text{H}]|$, while positive $dV_\phi/d[\text{Fe}/\text{H}]$ in the thick disc is a consequence of the inside-out formation.

Gradient inversions in $d[\text{Fe}/\text{H}]/dR$ and $dV_\phi/d[\text{Fe}/\text{H}]$, while caused by the inside-out formation, are not conditional to each other. In particular, the inverse relationship, $dV_\phi/d[\text{Fe}/\text{H}] > 0$, in the thick disc, just implies that for a specified metallicity range, more metal-poor stars formed at smaller radii, which is a characteristic of an IO-forming disc. However, inside-out formation does not have to invert $d[\text{Fe}/\text{H}]/dR$ in the stellar populations. We have shown that higher velocity dispersions for older populations act in opposite directions on the two statistics. While increased asymmetric drift, i.e. lower V_ϕ , gives a positive contribution to $dV_\phi/d[\text{Fe}/\text{H}]$, the associated radial expansion gives a negative contribution to $d[\text{Fe}/\text{H}]/dR$, helping to differentiate between the different factors at hand.

In higher precision data, the $V_\phi([\text{Fe}/\text{H}])$ for high $[\alpha/\text{Fe}]$ stars will be an important diagnostic for the formation of the Milky Way’s thick disc. As we showed in Fig. 11, the original radial metallicity gradient of the high $[\alpha/\text{Fe}]$ /thick disc directly imprints on $V_\phi([\text{Fe}/\text{H}])$: if $d[\text{Fe}/\text{H}]/dR$ is negative in the star-forming disc at that time, the knee in the $[\text{Fe}/\text{H}]-[\alpha/\text{Fe}]$ plane lies at lower $[\text{Fe}/\text{H}]$ for outer galactic radii, and hence $V_\phi([\text{Fe}/\text{H}])$ would decline towards larger metallicities after reaching a maximum. This is, however, a tricky measurement to make, since contamination of this sequence with the faster rotating lower $[\alpha/\text{Fe}]$ stars biases the metal-rich end towards larger V_ϕ , while decreasing disc contamination and increasing halo contamination exacerbate the decline of V_ϕ towards lower metallicities. Uncertain abundance errors, made worse by the common strategy to adopt a sample selection sloping in $[\alpha/\text{Fe}]$ versus $[\text{Fe}/\text{H}]$, make it difficult to judge the current survey results (this contamination problem is mentioned by Bekki & Tsujimoto 2011), but a notable decrease of V_ϕ towards larger $[\text{Fe}/\text{H}]$ in the high $[\alpha/\text{Fe}]$ subset of Wojno et al. (2016), which we tested to be similar to our models when folded with 0.2 dex errors, gives an interesting indication for a negative gradient in the past MW disc.

We also examined the consequences of the inside-out formation for $d[\text{Fe}/\text{H}]/dz$ in the disc. At the solar galactocentric radius, inside-out formation contributes of the order of ~ -0.2 dex kpc^{-1} to $d[\text{Fe}/\text{H}]/dz$, bringing the model in line with observed vertical metallicity age gradients, while fitting constraints for the vertical change in mean stellar age. We also note that the models predict flatter/more negative radial $d[\text{Fe}/\text{H}]/dR$ metallicity gradients at larger altitudes z . Testing against a model without radial migration reveals that the main driver for the change of radial gradients with altitudes is radial migration with the outwards increase of scaleheights under action conservation, with the contributing factor that the more metal-poor old inner disc populations become more dominant at high altitudes in the inner disc.

If a disc has a star-formation cut-off (steepening of the Kennicutt–Schmidt law below a threshold surface density), the shifts of the cut-off radius with time will affect the local metallicity gradients even more strongly than the classic inside-out formation. For example, an outwards shift of the cut-off radius at relatively early times (in particular if the disc has some radial mixing of the gas) will contribute very positively to $d[\text{Fe}/\text{H}]/dR$. Also, near the cut-off, the blurring term of radial mixing gains particular importance due to the strong radial density contrasts. We see this in our models, both in the metallicity gradients around the cut-off and

in the large effects on the vertical structure of the disc near that region.

While this paper helps to link and also differentiate these different observational findings, a quantitative study of these processes has to be left to specific modelling of each survey. We used a model that is largely consistent with the Milky Way, but has to be fitted in detail to the upcoming data. At the current stage, we cannot reliably derive tighter constraints on the inside-out formation time-scales. We have neither a good constraint on the enrichment time-scale of the system, as neither the Bensby, Feltzing & Oey (2014) sample offers the necessary precision at ages greater than ~ 10 Gyr, nor do we know e.g. the SNIa time-scales to sufficient precision to provide more than a rough estimate that the inside-out formation time-scale of the Milky Way should have been ~ 2 Gyr, comparable to the SNIa time-scale and the time-scale of initial metallicity enrichment. With all its quantitative uncertainties, this qualitative result can be considered robust.

Our models also underline the need for a better understanding of gas flows in galaxies. There are several processes that can produce inverse radial metallicity gradients in the star-forming ISM. The traditional explanations range from the piercing of cold accretion into the central galaxy (an explanation in the literature, which we consider less plausible) to intrinsic gradient inversions in classical chemical evolution models in the absence of flows, which we identify, however, with manual changes of the Schmidt–Kennicutt law of star formation. Instead, we suggest other natural explanations: (i) higher losses of processed material from the central regions, (ii) re-accretion of some of the enriched material in galactic fountain-ing, aided by the inside-out formation, that favours stronger relative accretion rates on outer radii, or (iii) a general outwards push of the enriched material, which would be natural, because high-angular momentum stellar yields push into the partially pressure- and turbulence-supported hot medium. Again, these processes will have to be differentiated and quantified in future models and comparisons with observations. All we can achieve here is pointing out the possibility and feasibility, and leave the quantification to future publications.

ACKNOWLEDGEMENTS

It is a pleasure to thank J. Binney for interesting discussions and helpful comments on the draft. We would like to thank M. Aumer, M. Bergemann, D. Kawata, G. Pezzulli and J. Stott for helpful comments. This work was partly supported by the European Union FP7 programme through European Research Council grant number 320360. PJM gratefully acknowledges financial support from the Swedish National Space Board and the Royal Physiographic Society in Lund.

REFERENCES

Aguirre A., Hernquist L., Schaye J., Katz N., Weinberg D. H., Gardner J., 2001, *ApJ*, 561, 521
 Andrews B. H., Weinberg D. H., Schönrich R., Johnson J., 2016, preprint (arXiv:1604.08613)
 Aumer M., Binney J., 2009, *MNRAS*, 397, 1286
 Aumer M., Binney J., Schönrich R., 2016, *MNRAS*, 459, 3326
 Bekki K., Tsujimoto T., *ApJ*, 738, 4
 Bensby T., Feltzing S., Oey M. S., 2014, *A&A*, 562, 71
 Bergemann M. et al., 2014, *A&A*, 565, 89
 Bilitewski T., Schönrich R., 2012, *MNRAS*, 426, 2266
 Binney J., McMillan P. J., 2011, 413, 1889
 Binney J., McMillan P. J., 2016, 456, 1982

Bird J., Kazantzidis S., Weinberg D., Guedes J., Callegari S., Mayer L., Madau P., 2013, *ApJ*, 773, 43
 Bland-Hawthorn J., Cohen M., 2003, *ApJ*, 582, 246
 Boeche C. et al., 2014, *A&A*, 568, 71
 Brook C. B., Stinson G., Gibson B. K., Roškar R., Wadsley J., Quinn T., 2012, *MNRAS*, 419, 771
 Casagrande L., Schönrich R., Asplund M., Cassisi S., Ramírez I., Meléndez J., Bensby T., Feltzing S., 2011, *A&A*, 530, 138
 Casagrande L. et al., 2016, *MNRAS*, 455, 987
 Chabrier G., 2003, *PASP*, 115, 763
 Cheng J. et al., 2012, *ApJ*, 746, 149
 Chiappini C., Matteucci F., Romano D., 2001, *ApJ*, 554, 1044
 Collins J. A., Shull J. M., Giroux M. L., 2009, *ApJ*, 657, 271
 Cresci G., Mannucci F., Maiolino R., Marconi A., Gnerucci A., Magrini L., 2010, *Nature*, 467, 811
 Curir A., Lattanzi M. G., Spagna A., Matteucci F., Murante G., Re Fiorentin P., Spitoni E., 2012, *A&A*, 545, 133
 Davé R. et al., 2001, *ApJ*, 552, 473
 Dehnen W., Binney J., 1998, *MNRAS*, 298, 387
 Flynn C., Holmberg J., Portinari L., Fuchs B., Jahrei H., 2006, *MNRAS*, 372, 1149
 Fox A. J. et al., 2016, *ApJ*, 816, 11
 Friedli D., Benz W., Kennicutt R., 1994, *ApJ*, 430, 105
 Genovali K. et al., 2015, *A&A*, 580, 17
 Gibson B. K., Pilkington K., Brook C. B., Stinson G. S., Bailin J., 2013, *A&A*, 554, 47
 Haywood M., 2008, *MNRAS*, 388, 1175
 Holmberg J., Flynn C., 2004, *MNRAS*, 352, 440
 Holmberg J., Nordström B., Andersen J., 2009, *A&A*, 501, 941
 Ivezić Z. et al., 2008, *ApJ*, 684, 287
 Jones T. A., Ellis R. S., Jullo E., Richard J., 2010, *ApJ*, 725, 176
 Jones T. A., Ellis R. S., Richard J., Jullo E., 2013, *ApJ*, 765, 48
 Jurić et al., 2008, *ApJ*, 673, 864
 Kawata D., Grand R., Gibson B., Casagrande L., Hunt J., Brook A., 2017, *MNRAS*, 464, 702
 Kordopatis G. et al., 2011, *A&A*, 535, 107
 Kordopatis G. et al., 2013, *MNRAS*, 436, 3231
 Lacey C. G., Fall S. M., 1985, *ApJ*, 290, 154
 Lee Y. S. et al., 2011, *ApJ*, 738, 187
 Loebman S., Roškar R., Debattista V., Ivezić Ž., Quinn T., Wadsley J., 2011, *ApJ*, 737, 8
 Luck R. E., Lambert D. L., 2011, *AJ*, 142, 136
 McKee C. F., Parravano A., Hollenbach D. J., 2015, *ApJ*, 814, 13
 McWilliam A., Matteucci F., Ballero S., Rich R., Fulbright J., Cescutti G., 2008, *AJ*, 136, 367
 Maeder A., 1992, *A&A*, 264, 105
 Marasco A., Fraternali F., Binney J., 2012, *MNRAS*, 419, 1107
 Marinacci F., Fraternali F., Nipoti C., Binney J., Ciotti L., Londrillo P., 2011, *MNRAS*, 415, 1534
 Meyer D. M., York D. G., 1987, *ApJ*, 315, 5
 Minchev I., Famaey B., Quillen A., Dehnen W., Martig M., Siebert A., 2012, *A&A*, 548, 127
 Minchev I., Chiappini C., Martig M., 2014, *A&A*, 572, 92
 Miranda M. S. et al., 2016, *ApJ*, 817, A10
 Nath B. B., Trentham N., 1997, *MNRAS*, 291, 505
 Pezzulli G., Fraternali F., 2016, *MNRAS*, 455, 2308
 Pezzulli G., Fraternali F., Boissier S., Muñoz-Mateos J. C., 2015, *MNRAS*, 451, 2324
 Piffl T. et al., 2014, *MNRAS*, 445, 3133
 Prantzos N., Boissier S., 2000, *MNRAS*, 313, 338
 Przybilla N., Nieva M.-F., Butler K., 2008, *ApJ*, 688, 103
 Queyrel J. et al., 2012, *A&A*, 539, 93
 Rahimi A., Kawata D., Allende-Prieto C., Brook C., Gibson B., Kiessling A., 2011, *MNRAS*, 415, 1469
 Rahimi A., Carrell K., Kawata D., 2014, *Res. Astron. Astrophys.*, 14, 1406
 Read J. I., 2014, *J. Phys. G: Nucl. Phys.*, 41, 063101
 Roškar R., Debattista V., Loebman S., 2013, *MNRAS*, 433, 976
 Rupke D. S. N., Kewley L. J., Barnes J. E., 2010, *ApJ*, 710, 156

- Salpeter E., 1955, *ApJ*, 121, 161
 Sanders J., Binney J., 2015, *MNRAS*, 449, 3479
 Schlesinger K. et al., 2014, *ApJ*, 791, 112
 Schönrich R., Binney J., 2009a, *MNRAS*, 396, 203 (SB09)
 Schönrich R., Binney J., 2009b, *MNRAS*, 399, 1145 (SB09b)
 Schönrich R., Binney J., 2012, *MNRAS*, 419, 1546
 Schönrich R., Binney J., Dehnen W., 2010, *MNRAS*, 403, 1829
 Sellwood J. A., Binney J. J., 2002, *MNRAS*, 336, 785
 Shopbell P. L., Bland-Hawthorn J., 1998, *ApJ*, 493, 129
 Shull J. M., Stevans M., Danforth C., Penton S. V., Lockman F. J., Arav N., 2016, *ApJ*, 739, 105
 Solway M., Sellwood J. A., Schönrich R., 2012, *MNRAS*, 422, 1363
 Spagna A., Lattanzi M. G., Re Fiorentin P., Smart R. L., 2010, *A&A*, 510, 4
 Spitoni E., Matteucci F., 2011, *A&A*, 531, 72
 Spitoni E., Recchi S., Matteucci F., 2008, *A&A*, 484, 743
 Stott J. P. et al., 2014, *MNRAS*, 443, 2695
 Tisserot F., Dauphas N., Grossman L., 2016, *Sci. Adv.*, 2, e1501400
 Tumlinson J. et al., 2011, *Science*, 338, 6058, 948
 Vera-Ciro C., D'Onghia E., Navarro J., Abadi M., 2014, *ApJ*, 794, 173
 Walch S. et al., 2015, *MNRAS*, 454, 238
 Wang J. et al., 2011, *MNRAS*, 413, 1373
 Wojno J. et al., 2016, *MNRAS*, 461, 4246
 Wuyts E. et al., 2016, *ApJ*, 827, 74
 Yuan T.-T., Kewley L. J., Swinbank A. M., Richard J., Livermore R. C., 2011, *ApJ*, 732, 14

APPENDIX A: EXAMINING THE EFFECTS OF A CHANGING CIRCULAR VELOCITY CURVE

The purpose of this appendix is to examine the effects of the changing potential associated with the growing galaxy, which causes adiabatic contraction. While the disc is accreting more mass, one would expect some increase in the circular speed, which leads to an adiabatic contraction of older disc populations.

There are two possible ways to think about this problem.

(i) A straightforward way is to use the fact that our problem is from the beginning formulated in the angular momentum $L_{z,0}$. The spatial dimension only enters in the chemical evolution model for assessing star formation and radial flows. However, the radial flows in the gas are at least an order of magnitude faster than the adiabatic contraction. The uncertainties in the time-dependent star formation efficiencies from the Schmidt–Kennicutt law are far larger than the associated corrections to the surface density – the adiabatic contraction looks from this perspective similar to a very minor addition to radial flows and a very slightly increased coefficient in the star formation efficiency. With this argumentation, we can argue that the treatment of adiabatic contraction is not relevant.

(ii) We can keep a fixed spatial interpretation of the chemical evolution model and impose a zeroth-order correction for changes of V_c by inserting an additional matrix for the adiabatic correction $A(R, L_{z,0}, t)$ that maps the original radius to the angular momentum $L_{z,0}$ in front of the churning matrix M . We will quickly move along this line of argumentation to give a rough estimate of the effect.

From Wang et al. (2011) and other cosmological simulations, we know that most of the inner halo is already in place before a disc can form. Also, the turbulent behaviour in the first period of mass accretion likely prevents the formation of a disc. Thus, most of the halo contribution should already be in place. For the sake of simplicity, we will assume for the halo/dark matter contribution to the circular speed:

$$V_{c,h}^2(t) = V_{c,h}^2(12 \text{ Gyr}) \cdot \left(\frac{3}{4} + \frac{1}{4} N \int_0^t I(t') dt' \right), \quad (\text{A1})$$

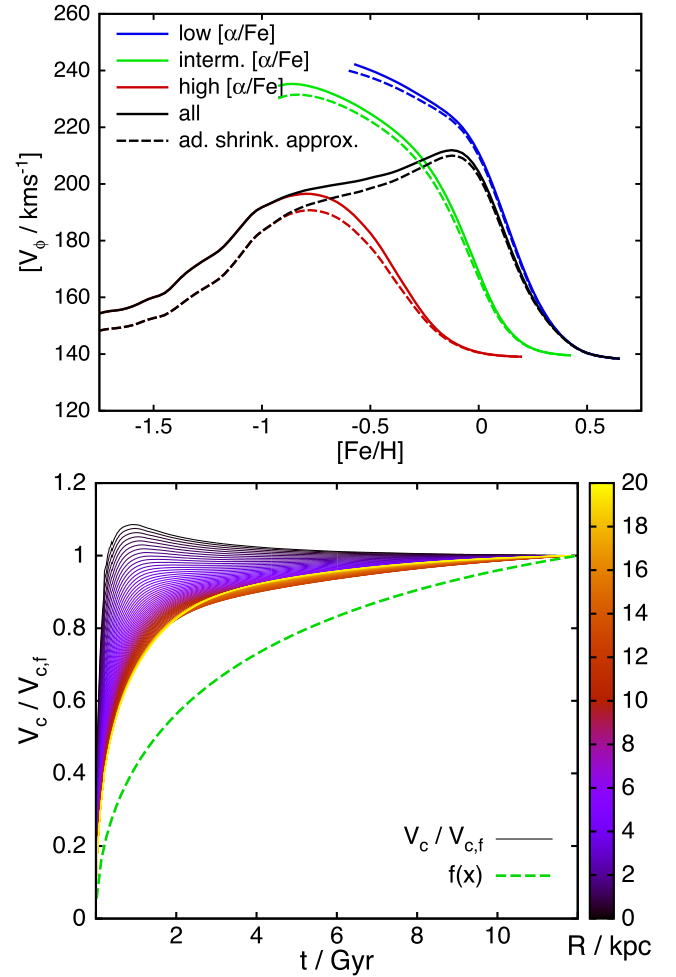


Figure A1. Effects of adiabatic contraction of the disc as the galaxy grows. The lower panel shows the value of the disc's contribution to V_c as a fraction of its final contribution, as a function of time. The different colours correspond to different radii. The green dashed line is the naive expectation from the gas accretion rate. The upper panel shows the minor effect of this growth on the $[\text{Fe}/\text{H}]$ – V_ϕ trends for different components in the inside-out formation model; see Fig. 11.

where I is the gas infall over time and $N = (\int_0^t I dt')^{-1}$. The square-root of the infall term is depicted with a green line in the bottom panel of Fig. A1. It would be tempting to use just the same term for the contribution for the galactic disc, but three factors lead to a fast, early increase of the circular speed in the disc. The square-root of the disc contribution as a function of radius and time is depicted with coloured lines in the bottom panel of Fig. A1. To get the approximation plotted here (which excludes effects of the changing scaleheight of the components), we calculated the circular speed contribution of the disc using the surface density profile of our disc and a fixed exponential vertical density profile with 300 pc scaleheight. We identify three reasons for this behaviour.

(i) The loss of material with star formation means that a somewhat higher fraction of the final mass than one would expect accumulates in the early history of the galaxy. Intuitively, this is also rooted in the first build-up of the gas disc and its subsequent decline in mass.

(ii) The inside-out formation leads to a far quicker accumulation of mass in the inner radii, moving the increase in circular speed

particularly in the inner parts, but also further out, to far earlier times

(iii) The disc mass distribution is far from spherical, and hence the radial surface density gradient near each point contributes significantly to the radial force. That is, a steeper radial surface density gradient will deliver a significant positive contribution to the circular velocity. The increasing scalelength of the disc hence gives a decreasing contribution to $V_c(R, t)$ over time and can even dominate in the inner disc, as we see from Fig. A1.

We note that an increase in scaleheight over time would yield a minor effect in the same direction, and a bulge would limit adiabatic contraction further. We now add our two approximate terms for disc and halo with weights 0.6 and 0.4 together, to obtain

$$V_c^2(t) = V_{c,h}^2(t) + V_{c,d}^2(t), \quad (\text{A2})$$

and calculate, from this term, the transition matrix A . The effect of this change on the $[\text{Fe}/\text{H}]-v_\phi$ relationships for different components of our model with the inside-out formation is shown in Fig. A1 (compare to Fig. 11, top panel). As expected, the effect of the adiabatic contraction (compare the dashed lines to the solid lines) is very minor, primarily causing a small decrease of the average azimuthal velocity for lower metallicity stars.

This paper has been typeset from a $\text{\TeX}/\text{\LaTeX}$ file prepared by the author.